Chalise *et al.*
EURASIP Journal on Advances in Signal Processing (2023) 2023:14
https://doi.org/10.1186/s13634-022-00967-z

EURASIP Journal on Advances in Signal Processing

RESEARCH Open Access

Information embedding in DFRC networks through chirp waveform diversity

Batu K. Chalise[1*], Moeness G. Amin[2] and Giuseppe A. Fabrizio[3]

*Correspondence:
bchalise@nyit.edu

[1] Department of Electrical and Computer Engineering, New York Institute of Technology, Old Westbury, NY, USA
[2] Center for Advanced Communications, Villanova University, Villanova, PA, USA
[3] Defence Science and Technology Group, Department of Defence, Adelaide, Australia

Abstract

We consider a dual function radar communications network and propose a waveform diversity-based approach to embed both target and scheduling data in the transmitter pulses. The scheduling data of radar signal bandwidth, carrier frequency, and waveform along with the information on target detection, range, and Doppler are shared among the network radar nodes without a need for designated communication links. Scheduling and target information are encoded to bits and transmitted over the radar coherent processing interval using up- and down-chirps. We derive exact expressions of probability of bit error and false alarm rate for sharing scheduling and target information data between two radar nodes. The effect of different parameters and data sharing on the radar performance is analyzed and validated by computer simulations. Using the cross-ambiguity function, we show the capability of the up- and down- chirp sequence transmission scheme in reducing range sidelobes compared to the conventional transmission of only the up- (or down-) chirps. To overcome the limited data rate associated with only using two chirp waveforms, we consider orthogonal chirp division multiplexing and derive its CAF. We demonstrate the suitability of OCDM for high data rate radar operations by examining the mainlobe width and sidelobe levels of the zero-Doppler and zero-delay cuts of the CAF.

Keywords: Dual function radar and communications, Chirp-based waveform diversity, Scheduling and target related information, Up- and down- chirps, Orthogonal chirp division multiplexing

1 Introduction

Radio frequency (RF) coexistence permits spectrum sharing between separately developed radar and communications systems by avoiding or significantly reducing the mutual interference [1–7]. Different coexistence strategies require different levels of cooperation or coordination between the two RF systems [8, 9]. The ultimate coordination is reached when the two systems share the same platform, which is commonly referred to as dual function radar and communications (DFRC) systems [10–14]. The DFRC platforms, when radar is the legacy system, aim at enabling communications to capitalize on the radar resources and infrastructure, while striving to be transparent to radar operations and mission. It does so by embedding information intended for communications receivers into the radar waveforms intended for radar receivers. In essence,

in DFRC systems, the communications part does not need not to have a designated RF link and is allowed to benefit from the radar's large bandwidth, transmit power, antenna gains, and high-quality hardware.

This paper considers dual system functionality in radar networks where communication signal embedding in radar waveforms is for the sole purpose of assisting and enhancing the radar network functionality. This principal feature defines a specific class of dual function systems in which communications is an integral part of the radar and is considered essential for its successful execution and completion. This class can be applied to monostatic, bi-static, and multi-static radar configurations. The embedded information can be scheduling, including the radar parameters planned over the next coherent processing interval (CPI), and/or sensing which consists of the learned target characteristics, such as range, angle, and Doppler. For example, scheduling information such as bandwidth used by one radar node is a crucial information for another node to avoid collision and minimize the effects of inter-node interference. Similarly, a radar node can share, with another radar, its target related information, such as the value of the likelihood ratio test function which is pertinent to the presence or absence of target in each range cell. This approach seeks to assist a low performance radar node to improve its target detection capability.

There are three main strategies introduced for embedding communication signals in radar parameters, where radar is considered the legacy system. In principle, a radar system can change its beam, its fast time waveform, or its slow time waveform according to the communication symbols. Signal embedding through modulations of the radar beam is referred to as sidelobe signal embedding [15, 16]. This technique modifies the optimally designed radar beam and assumes precise values of the sidelobes which is difficult to attain. Further, radar beam-based embedding is generally suitable for only low data rates and small size constellations. Signal embedding over fast time achieves much higher data rates than beam and sidelobe modulations, and it is referred as intrapulse modulation [17–23]. This type of embedding can be performed using eigenvectors-based methods, weighted-combining, and dominant-projection techniques [17]. Binary phase shift keying (BPSK), quadrature phase shift keying (QPSK), and multilevel M-ary PSK can also be used to remodulate the radar waveforms. However, any effort to remodulate the radar waveform is deemed to change its characteristics, the degree of which depends on the embedded bit rate and the modulation type. Remodulation can also increase security risks, for example, constant BPSK sampling rate can be easily detected by the cyclostationary analysis [24], which the eavesdropper can exploit to decode the embedded information. Multiple-input multiple-output (MIMO) radars have the additional option of utilizing the transmitted orthogonal waveforms in signal embedding and were considered in the context of DFRC systems [25–30]. On the other hand, dual function system in the context of passive radars was discussed in [31–33].

In order to avoid radar signal and beam remodulations, code-shift keying (CSK) strategies were proposed in which waveform diversity is utilized to embed information messages over the radar slow time [34]. A key aspect of this method is not to remodulate the radar waveform, but rather exploit diverse radar waveforms to carry information. In a radar network setting, CSK signaling using two diverse radar waveforms of up- and down- chirps was applied to communicate between two different radars [35, 36]. The bit

error rate (BER) expression was derived incorporating the waveform correlation coefficient. However, the analysis was limited to a case in which signal processing at the radar receiver is applied to individual CPIs. Although this approach seems reasonable since each pulse carries a certain bit (group of bits) of information, deciphering information over the radar CPI was not applied. The scheme was extended in [37] to a case in which multiple pulses are processed to achieve CPI gain for detection. The authors proposed analytical approach for performance analysis and examined the effect of different parameters on the achieved communication and radar performance. However, the approach was based on simplified system model assumptions, limited to only up- and down- chirps, and did not consider corresponding cross-ambiguity function (CAF) analysis and high data rate transmissions with orthogonal chirp division multiplexing (OCDM) approach.

1.1 Contributions

In this paper, we propose a novel analytical framework to derive an exact expression of the probability of bit error, and exact and approximate expressions of the probabilities of false alarm (PFA) and detection, respectively, for the case of sharing scheduling data and target information between two radar nodes. We verify their accuracy and demonstrate the effect of different parameters on the performance of communications and radar. The effectiveness of the proposed up- and down- chirp sequence transmission in reducing range sidelobe levels, compared to the conventional transmission of only the up- (or down-) chirps, is demonstrated by analyzing the CAF. To overcome the limited information rate transmission capability of up- and down-chirps, we propose orthogonal chirp division multiplexing (OCDM) approach as a new approach for embedding information at higher data rates. To the best of our knowledge, the suitability of the OCDM for radar operations has not been investigated before in the literature. Toward this end, we derive CAF of the OCDM signal and demonstrate that it improves both zero-Doppler and zero-delay cuts of the CAF in terms of their mainlobe width and peak-to-sidelobe ratio (PSR).

The remainder of this paper is organized as follows. The proposed system model is discussed in Sect. 2. The performance analysis of information embedding with up- and down- chirps is provided in Sect. 3. The CAF of a sequence of up- and down- chirps is derived in Sect. 4. Section 5 proposes OCDM method and derives the CAF of OCDM signal. Simulation results are presented in Sect. 6 and conclusions are drawn in Sect. 7.

1.2 Notations

Upper (lower) bold face letters will be used for matrices (vectors); $(\cdot)^*$, $(\cdot)^H$, $\mathbf{I}$, $||\cdot||$ will denote complex conjugate, Hermitian transpose, identity matrix, Euclidean norm for vector; $f_X(x)$, $F_X(x)$, and $\Pr\{\cdot\}$ will denote probability density function (PDF), cumulative distribution function (CDF), and the probability operator, respectively. $\mathcal{N}_C(0,\sigma^2)$ and $\mathbb{X}_n^2(a)$ denote circularly symmetric complex Gaussian (CSCG) distribution and chi-squared distribution with n degrees of freedom and mean a, respectively. $\Gamma(\alpha)$, $\gamma(\alpha,z)$, and $\Gamma(\alpha,z)$ denote the Gamma function, lower incomplete Gamma function, and upper incomplete Gamma function, respectively.

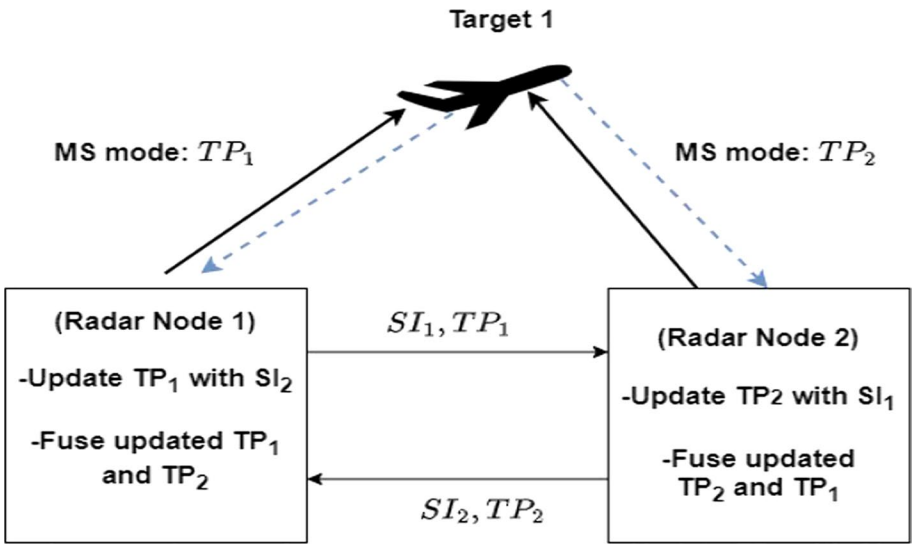

Fig. 1 Schematic of information embedding through waveform diversity in radar network

2 System model

A schematic diagram of information embedding in a radar network with waveform diversity concept is shown in Fig. 1. Radar nodes 1 and 2 cooperate to enhance target detection and parameter estimation by sharing target and scheduling information (e.g., bandwidth, waveforms, and array configuration of each radar) as follows. Each radar transmits its current scheduling information (SI) and target parameters (TP) acquired through monostatic (MS) operation mode during previous CPI, employing waveform diversity concept. A typical and simple example of waveform diversity is transmitting up-chirp to carry information bit 1 and down-chirp to carry information 0. Each bit may represent a message on its own. For example, for scheduling information, bit 1 can indicate that the pulse repetition interval (PRI) is above a certain value and bit 0 would represent otherwise. Similarly, for target information, bit 1 may indicate that the estimated range of a target is above 50 Km and bit 0 may indicate the opposite. In either case, more elaborate and accurate information would naturally require more bits, which can be achieved with the OCDM that allows transmission of bits or symbols with orthogonal chirps. Since target and scheduling information are typically assumed to remain constant over a CPI, they can be encoded in a number of bits equal to or less than that of a CPI. It is also worth noting that during a current CPI, the embedded scheduling information represents what the radar plans to use in the next CPI, whereas the target information represents what the radar extracted in the previous CPI. Radar node 1 then estimates SI_2 and TP_2, reacquires (updates) TP_1 with the knowledge of SI_2, and then fuses the updated TP_1 with TP_2 to obtain improved target parameter estimates. On the other hand, Radar 2 estimates SI_1 and TP_1, reacquires (updates) TP_2 with the knowledge of SI_1, and then fuses the updated TP_2 with TP_1 to obtain its improved target parameter estimates. The process can be generalized for the cases with multiple targets as well as the case with more than two nodes. The target parameter estimates are then ultimately fused to obtain tracks associated with each target, which allows discerning an overall surveillance picture. Although incorporating all of these steps into a common analytical

framework is an interesting future work, in this paper, we focus on one specific aspect which is acquiring target parameter and decoding scheduling information using different types of information embedded chirp signals.

Typically, scheduling data and target information can be encoded with two different schemes as proposed in [36]. The first scheme encodes different information into bits, one parameter at a time, i.e., performing sequential encoding or embedding. The values assumed by each radar or target parameter form a constellation, or a dictionary on its own. The second scheme uses only one scheduling data constellation or dictionary whose size is determined by the product of the constellation sizes of all symbols. Each combination of the values of the different parameters defines one symbol of the scheduled data constellation, and is represented by a binary sequence whose length is equal to the number of pulses in the CPI. The number of bits required for the second scheme is always less than or at most equal to the number of bits required in the first scheme. However, if there is a bit error in the second scheme, the whole message becomes incorrect. For both encoding schemes, the probability of error in information decoding can be determined from the probability of bit error. Therefore, in the following section we will derive this bit error probability including radar performance metrics.

3 Scheduling information transfer with up- and down-chirps

We consider a dual function radar that sends up- and down- chirps carrying bits 1 and 0, respectively[1]. These chirp signals can be expressed as

$$s_u(t) = \frac{1}{\sqrt{T}}\text{rect}\left(\frac{t}{T}\right)e^{j(2\pi f_0 t+\pi\alpha t^2)},\ \ s_d(t) = \frac{1}{\sqrt{T}}\text{rect}\left(\frac{t}{T}\right)e^{j(2\pi f_0 t-\pi\alpha t^2)}, \tag{1}$$

where f_0 is the carrier frequency, $\alpha = \frac{B}{T}$ is the chirp slope, T is the pulse width, B is the waveform bandwidth, and $\text{rect}\left(\frac{t}{T}\right)$ denotes the rectangular function defined as $\text{rect}\left(\frac{t}{T}\right) = 1$, for $-\frac{T}{2} \le t \le \frac{T}{2}$ and $\text{rect}\left(\frac{t}{T}\right) = 0$, for any other t. $s_u(t)$ and $s_d(t)$ are normalized such that

$$\int_{-\infty}^{\infty} s_u(t)s_u^*(t)\,dt = \int_{-\infty}^{\infty} s_d(t)s_d^*(t)\,dt = 1. \tag{2}$$

The cross correlation between $s_u(t)$ and $s_d(t)$ can be expressed as

$$\beta = \int_{-\infty}^{\infty} s_u^*(t)s_d(t)\,dt = \frac{1}{T\sqrt{\alpha}}\left[C(\sqrt{\alpha}T) + jS(\sqrt{\alpha}T)\right], \tag{3}$$

where $C(\sqrt{\alpha}T)$ and $S(\sqrt{\alpha}T)$ are the cosine and sine Fresnel functions defined as

$$C(\sqrt{\alpha}T) = \int_0^{\sqrt{\alpha}T} \cos\left(\frac{\pi t^2}{2}\right)dt,\ \ S(\sqrt{\alpha}T) = \int_0^{\sqrt{\alpha}T} \sin\left(\frac{\pi t^2}{2}\right)dt. \tag{4}$$

[1] The idea of using LFM waveforms to represent digital information was first proposed in [38].

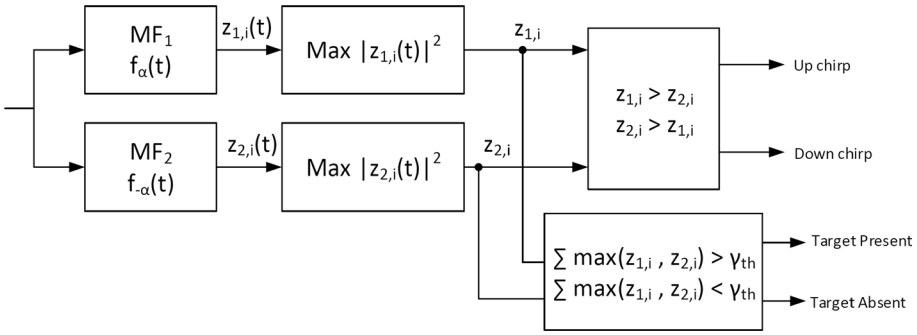

Fig. 2 Information decoding and detection using waveform diversity

Note that $C(\sqrt{\alpha}T)$ and $S(\sqrt{\alpha}T)$ converge to 0.5 for high values of $\sqrt{\alpha}T$ [35]. After down-conversion, the received signal can be expressed as[2]

$$y(t) = \begin{cases} \alpha_t s_u(t-\tau_d) + n(t), & \text{if up chirp was sent,} \\ \alpha_t s_d(t-\tau_d) + n(t), & \text{if down chirp was sent,} \end{cases}$$

where τ_d is time-delay, α_t is channel/path attenuation[3] which, depending on monostatic/bi-static configuration, includes the effects of transmitted power, transmit and receive antenna gains, target radar cross-section (RCS), and monostatic/bi-static ranges [39]. $n(t)$ is additive Gaussian noise, which is assumed to have zero-mean and variance σ_n^2.

Radar node 1 transmits L up-chirps/down-chirps within each CPI, depending on the scheduling and/or target information bits. Radar node 2 (see Fig. 2) receiver, unaware of the pulse transmitted, consists of two matched-filters (MFs). One filter is matched to the waveform $s_u(t)$, whereas the other is matched to the waveform $s_d(t)$. Let $z_{1,i}(t)$ and $z_{2,i}(t)$ represent the outputs of the filters corresponding to the i-th pulse. Define $t_1 = \arg\max_t |z_{1,i}(t)|^2$ and $t_2 = \arg\max_t |z_{2,i}(t)|^2$. Except in very low signal-to-noise ratio (SNR) regime, t_1 will approximate τ_d if the received signal consists of an up-chirp and t_2 will approximate τ_d if the received signal consists of a down-chirp. Assuming that this approximation is accurate, and compensating for the delay, the sampled (discrete) outputs of the two filters for the ith pulse can be expressed as

$$z_{1,i} = \mathbf{s}_u^H \mathbf{y}_i = \alpha_t \mathbf{s}_u^H \mathbf{s}_i + \mathbf{s}_u^H \mathbf{n}_i, \;\; z_{2,i} = \mathbf{s}_d^H \mathbf{y}_i = \alpha_t \mathbf{s}_d^H \mathbf{s}_i + \mathbf{s}_d^H \mathbf{n}_i, \tag{5}$$

where $\mathbf{y}_i = [y_i(0), \ldots, y_i(L_c-1)]^T$ and $\mathbf{n}_i = [n_i(0), \ldots, n_i(L_c-1)]^T$ denote the sampled versions of the received signal $y(t)$ and noise $n(t)$ during the ith pulse. Similarly, $\mathbf{s}_i = [s_i(0), \ldots, s_i(L_c-1)]^T$ is the sampled version of the waveform $s_i(t)$, which can be either $\mathbf{s}_u = [s_u(0), \ldots, s_u(L_c-1)]^T$ or $\mathbf{s}_d = [s_d(0), \ldots, s_d(L_c-1)]^T$ (the sampled versions of up-chirp and down-chirp, respectively). Here, $y_i(l)$, $n_i(l)$, $s_i(l)$, $s_u(l)$, and $s_d(l)$ represent the lth samples of the vectors $\mathbf{y}_i$, $\mathbf{n}_i$, $\mathbf{s}_i$, $\mathbf{s}_u$, and $\mathbf{s}_d$, respectively. L_c is the number of samples per pulse so that $L_c T_s = T$, where T_s is the sampling period. Note that

[2] We consider that inter-node interference can be avoided because each node has scheduling information from other nodes.

[3] In the presence of non-fluctuating target, α_t is given by radar range equation [39], whereas in the absence of target and non-fading channel, it is given by Friis transmission equation.

$\mathbf{s}_u^H \mathbf{s}_u = \mathbf{s}_d^H \mathbf{s}_d = 1$, and $\beta = \mathbf{s}_u^H \mathbf{s}_d$. In the case of imperfect delay estimation by L_e samples, (5) can be expressed as

$$z_{1,i} = \mathbf{s}_u^H \bar{\mathbf{y}}_i, \;\; z_{2,i} = \mathbf{s}_d^H \bar{\mathbf{y}}_i, \tag{6}$$

where $\bar{\mathbf{y}}_i = [\bar{y}_i(0), \ldots, \bar{y}_i(L_e - 1), y_i(0), \ldots, y_i(L_c - L_e - 1)]$, and $[\bar{y}_i(0), \ldots, \bar{y}_i(L_e - 1)$ correspond to noise samples.

3.1 Performance analysis

In this section, we first analyze the performance of communications component of the DFRC network in terms of the BER, and then analyze target detection performance in terms of PFA and probability of detection.

3.1.1 Unified approach for probability of bit error

A bit error occurs if the detected pulse contains *up-chirp*, but the amplitude of the output of the filter matched to the *down-chirp* exceeds the output of the filter matched to the *up-chirp* and vice versa. The bit error probability can be expressed as

$$\begin{aligned} P_b =& \Pr\{\mathbf{y}^H \mathbf{s}_u \mathbf{s}_u^H \mathbf{y} \le \mathbf{y}^H \mathbf{s}_d \mathbf{s}_d^H \mathbf{y} | \mathbf{y} = \mathbf{y}_u\} \Pr\{\mathbf{y} = \mathbf{y}_u\} + \\ & \Pr\{\mathbf{y}^H \mathbf{s}_d \mathbf{s}_d^H \mathbf{y} \le \mathbf{y}^H \mathbf{s}_u \mathbf{s}_u^H \mathbf{y} | \mathbf{y} = \mathbf{y}_d\} \Pr\{\mathbf{y} = \mathbf{y}_d\}. \end{aligned} \tag{7}$$

Assuming that bits ones and zeros, i.e., up- and down- chirps are transmitted with equal probability, then $\Pr\{\mathbf{y} = \mathbf{y}_u\} = \Pr\{\mathbf{y} = \mathbf{y}_d\} = \frac{1}{2}$. Therefore, the probability of bit error can be expressed as

$$P_b = \frac{1}{2}\left[\Pr\left\{ \frac{\mathbf{y}_u^H \mathbf{s}_u \mathbf{s}_u^H \mathbf{y}_u}{\mathbf{y}_u^H \mathbf{s}_d \mathbf{s}_d^H \mathbf{y}_u} \le 1 \right\} + \Pr\left\{ \frac{\mathbf{y}_d^H \mathbf{s}_d \mathbf{s}_d^H \mathbf{y}_d}{\mathbf{y}_d^H \mathbf{s}_u \mathbf{s}_u^H \mathbf{y}_d} \le 1 \right\} \right]. \tag{8}$$

Note that $\mathbf{s}_u$ and $\mathbf{s}_d$ are deterministic and the eigenvalues of $\mathbf{s}_u \mathbf{s}_u^H$ and $\mathbf{s}_d \mathbf{s}_d^H$ are equal. Moreover, we assume that the target is non-fluctuating and the statistics of noise does not change over coherent pulse integration period. Due to these reasons, the two probability terms in (8) are equal. Therefore, (8) can be expressed as

$$P_b = \Pr\left\{ \frac{\mathbf{y}_u^H \mathbf{s}_u \mathbf{s}_u^H \mathbf{y}_u}{\mathbf{y}_u^H \mathbf{s}_d \mathbf{s}_d^H \mathbf{y}_u} \le 1 \right\}. \tag{9}$$

The expression in (9) is equivalent to deriving the CDF of the ratio of quadratic forms in complex Gaussian random vector, $\mathbf{y}_u = \alpha_t \mathbf{s}_u + \mathbf{n}$, with mean $\alpha_t \mathbf{s}_u$ and covariance matrix $\sigma_n^2 \mathbf{I}$, where σ_n^2 is the variance of elements of noise $\mathbf{n}$. This derivation is not trivial, and is often analytically intractable, mainly due to the dependence of numerator and denominator quadratic forms on the same random vector. One approach to deal with this ratio of the quadratic functions of non-zero mean Gaussian random vectors is to express it as a weighted (weights can be negative as well) sum of the non-central Chi-square distributed random variables. However, the CDF of such a ratio can only be obtained in terms of an integral of a complicated function that requires numerical computation [40]. Below, we propose a novel approach which does not require this numerical integration. Toward this end, we derive an exact expression for P_b as follows.

Proposition 1 *The probability of bit error, P_b, can be expressed as*

$$P_b = \Pr\left\{ \frac{|\tilde{n}_1 + \tilde{b}_1|^2}{|\tilde{n}_2 + \tilde{b}_2|^2} \leq 1 \right\}, \tag{10}$$

where $\tilde{n}_1 \sim \mathcal{N}_C(0,1)$, $\tilde{n}_2 \sim \mathcal{N}_C(0,1)$, $\tilde{b}_1 = \tilde{\mathbf{b}}(1)$, $\tilde{b}_2 = \tilde{\mathbf{b}}(2)$, $\tilde{\mathbf{b}} = \frac{\alpha_t}{\sigma_n}\mathbf{U}^H\mathbf{s}_u$. Here, $\mathbf{U}$ is the matrix of eigenvectors of $\mathbf{s}_u\mathbf{s}_u^H - \mathbf{s}_d\mathbf{s}_d^H$ arranged in the descending order with respect to its non-zero eigenvalues.

1 ***Proof***

Refer to Appendix A.

Let $X \triangleq |\tilde{n}_1 + \tilde{b}_1|^2$ and $Y \triangleq |\tilde{n}_2 + \tilde{b}_2|^2$. Since $\tilde{n}_1$ and $\tilde{n}_2$ are statistically independent CSCG, the random variables X and Y are independent non-central Chi-square distributed with the degrees of freedom 2, and means $2|\tilde{b}_1|^2$ and $2|\tilde{b}_2|^2$, respectively, i.e., $X \sim \mathbb{X}_2^2(2|\tilde{b}_1|^2)$ and $Y \sim \mathbb{X}_2^2(2|\tilde{b}_2|^2)$. The bit error probability can be re-expressed as

$$P_b = \Pr\left\{ \frac{X}{Y} \leq 1 \right\}. \tag{11}$$

The distribution of $\frac{X/2}{Y/2}$ follows a doubly non-central F-distribution [41]. □

Lemma 1 *The CDF of the random variable Z, $Z = \frac{X_1/n_1}{X_2/n_2}$, where $X_1 \sim \mathbb{X}_{n_1}^2(\lambda_1)$ and $X_2 \sim \mathbb{X}_{n_2}^2(\lambda_2)$, is given by*

$$F_Z(z) = \sum_{k=0}^{\infty}\sum_{l=0}^{\infty} \frac{\left(\frac{n_1 z}{n_2}\right)^{k+\frac{n_1}{2}} \lambda_1^k \lambda_2^l \, {}_2F_1\left(k + \frac{n_1}{2}, k + l + \frac{n_1+n_2}{2}; k + 1 + \frac{n_1}{2}; -\frac{n_1 z}{n_2}\right)}{2^{k+l-1} e^{\frac{\lambda_1+\lambda_2}{2}} (2k + n_1) B\left(\frac{n_1}{2} + k, \frac{n_2}{2} + l\right) k! l!}. \tag{12}$$

where ${}_2F_1(a, b; c; x)$ denotes Gauss hypergeometric function and $B(x, y)$ denotes Beta function [42].

Using **Lemma** 1*, the probability of bit error, $P_b = \Pr\left\{ Z \triangleq \frac{X/2}{Y/2} \leq 1 \right\}$, can be expressed as*

$$P_b = \sum_{k=0}^{\infty}\sum_{l=0}^{\infty} \frac{z^{k+1} \lambda_1^k \lambda_2^l \, {}_2F_1(k+1, k+l+2; k+2; -z)}{2^{k+l-1} e^{\frac{\lambda_1+\lambda_2}{2}} (2k+2) B(k+1, l+1) k! l!}. \tag{13}$$

It is worth noting that (13) *holds true also for the signal model* (6)*, i.e., when delay cannot be perfectly estimated. Moreover, although* (13) *includes double-summation of infinite series, we will observe in Sect.* 6 *that this series converges within a small number of terms.*

3.1.2 Detection performance

In conventional radar only system, target is considered to be detected if the amplitude of the matched-filtered output signal in a given range-cell is above a certain threshold. However, in the proposed DFRC, the task is to determine whether the pulse is up-chirp

or down-chirp before comparing the matched-filtered output signal amplitude with the threshold. Since $|\beta|$ may not be perfectly zero ($|\beta| = 0$ is the best case for correct waveform classification), the received signal can contain target signal even if waveforms are miss-classified. To provide better insights on the detection performance in a general case of a CPI with L pulses, we first determine performance metric for a single pulse and then generalize it to multiple pulses. Under correct classification of waveforms, the detection probability can be expressed as

$$\begin{aligned}\bar{P}_{D,1} =& \Pr\left\{|\mathbf{s}_u^H\mathbf{y}|^2 \geq \gamma_{\text{th}}, |\mathbf{s}_u^H\mathbf{y}|^2 \geq |\mathbf{s}_d^H\mathbf{y}|^2 \;\middle|\; \mathbf{y} = \mathbf{y}_u\right\}\Pr\{\mathbf{y} = \mathbf{y}_u\} \\ &+ \Pr\left\{|\mathbf{s}_d^H\mathbf{y}|^2 \geq \gamma_{\text{th}}, |\mathbf{s}_d^H\mathbf{y}|^2 \geq |\mathbf{s}_u^H\mathbf{y}|^2 \;\middle|\; \mathbf{y} = \mathbf{y}_d\right\}\Pr\{\mathbf{y} = \mathbf{y}_d\},\end{aligned} \tag{14}$$

where γ_{th} is the threshold value. Assuming equal probability of transmission of ones and zeros, then $\Pr\{\mathbf{y} = \mathbf{y}_u\} = \Pr\{\mathbf{y} = \mathbf{y}_d\} = \frac{1}{2}$, and due to symmetry of the remaining probability terms in (14), we obtain

$$\bar{P}_{D,1} = \Pr\left\{|\mathbf{s}_u^H\mathbf{y}_u|^2 \geq \gamma_{\text{th}}, |\mathbf{s}_u^H\mathbf{y}_u|^2 \geq |\mathbf{s}_d^H\mathbf{y}_u|^2|\right\}. \tag{15}$$

Similarly, under miss-classification case, the detection probability can be expressed as

$$\begin{aligned}\bar{P}_{D,2} =& \Pr\left\{|\mathbf{s}_d^H\mathbf{y}|^2 \geq \gamma_{\text{th}}, |\mathbf{s}_d^H\mathbf{y}|^2 \geq |\mathbf{s}_u^H\mathbf{y}|^2 \;\middle|\; \mathbf{y} = \mathbf{y}_u\right\}\Pr\{\mathbf{y} = \mathbf{y}_u\} + \\ &\Pr\{\mathbf{y} = \mathbf{y}_d\}\Pr\left\{|\mathbf{s}_u^H\mathbf{y}|^2 \geq \gamma_{\text{th}}, |\mathbf{s}_u^H\mathbf{y}|^2 \geq |\mathbf{s}_d^H\mathbf{y}|^2 \;\middle|\; \mathbf{y} = \mathbf{y}_d\right\},\end{aligned} \tag{16}$$

which, as in the case of correct classification of waveforms, can be simplified to

$$\bar{P}_{D,2} = \Pr\left\{|\mathbf{s}_d^H\mathbf{y}_u|^2 \geq \gamma_{\text{th}}, |\mathbf{s}_d^H\mathbf{y}_u|^2 \geq |\mathbf{s}_u^H\mathbf{y}_u|^2\right\}. \tag{17}$$

Without loss of generality, the total detection probability, $\bar{P}_D = \bar{P}_{D,1} + \bar{P}_{D,2}$, can be expressed as

$$\bar{P}_D = \Pr\left\{\max\left(|\mathbf{s}_u^H\mathbf{y}|^2, |\mathbf{s}_d^H\mathbf{y}|^2\right) \geq \gamma_{\text{th}}\right\}. \tag{18}$$

For L pulses, the above detection probability can be generalized to

$$\bar{P}_D = \Pr\left\{\sum_{i=1}^{L} \max\left(|\mathbf{s}_u^H\mathbf{y}_i|^2, |\mathbf{s}_d^H\mathbf{y}_i|^2\right) \geq \gamma_{\text{th}}\right\}. \tag{19}$$

The detection probability is a function of unknown threshold, γ_{th}, which can be determined for a given requirement on PFA. The false alarm occurs when the power of the matched filter output is above a certain threshold, γ_{th}, if the received signal does not contain reflection from the target, i.e., when $\mathbf{y}_i = \mathbf{n}_i$.

$$P_f = \Pr\left\{\sum_{i=1}^{L} \max\left(|\mathbf{s}_u^H\mathbf{n}_i|^2, |\mathbf{s}_d^H\mathbf{n}_i|^2\right) \geq \gamma_{\text{th}}\right\}. \tag{20}$$

Considering that the sum of (15) and (17) is equivalent to (18) and following similar steps as in Appendix-A, P_f can be expressed as

$$P_f = \Pr\left\{\sum_{i=1}^{L} \max\left(X_i, Y_i\right) \geq \frac{2\gamma_{\text{th}}}{\sigma_n^2}\right\}, \tag{21}$$

where $X_i = |\bar{n}_{1,i}|^2$ and $Y_i = |\bar{n}_{2,i}|^2$ are exponentially distributed random variables with the parameter $\frac{1}{2}$, i.e., their PDFs are given by $f_{X_i}(x_i) = \frac{1}{2}e^{-\frac{x_i}{2}}$ and $f_{Y_i}(y_i) = \frac{1}{2}e^{-\frac{y_i}{2}}$, respectively.

Proposition 2 *The PFA of* (20) *can be expressed in integral form as*

$$P_f = 1 - \int_0^{\frac{2\gamma_{\text{th}}}{\sigma_n^2}} \frac{e^{-\frac{z}{2}} z^{2L-1}}{2^L \Gamma(2L)} \, {}_1F_1\left(L; 2L; -\frac{z}{2}\right) dz, \tag{22}$$

and in terms of confluent hypergeometric function of two variables as

$$P_f = 2^L B(L,L)\left[2^{-L} - \sum_{m=0}^{2L-1} \frac{\gamma_{\text{th}}^m}{\sigma_n^{2m} m!} \Phi_1\left(L, 2L-m, 2L, -\frac{\gamma_{\text{th}}}{\sigma_n^2}, -1\right)\right], \tag{23}$$

where ${}_1F_1(\,)$ *and* $\Phi_1(\,)$ *are confluent hypergeometric functions of one and two variables* [42], *respectively.*

1 ***Proof***

Refer to Appendix B.

Since PFA can be efficiently computed using (22) or (23), the value of the threshold $\bar{\gamma}_{\text{th}} \triangleq \frac{2\gamma_{\text{th}}}{\sigma_n^2}$ for a given required PFA, P_f, can be obtained. After determining the threshold for a given PFA, we now proceed to analyze the detection probability in (19). Define $\bar{Z}_i \triangleq \max(|\mathbf{s}_u^H \mathbf{y}_i|^2, |\mathbf{s}_d^H \mathbf{y}_i|^2)$, whose CDF $F_{\bar{Z}_i}(\bar{z}_i) = \Pr\{\max(|\mathbf{s}_u^H \mathbf{y}_i|^2, |\mathbf{s}_d^H \mathbf{y}_i|^2) \leq \bar{z}_i\}$ can be expressed as

$$\begin{aligned} F_{\bar{Z}_i}(\bar{z}_i) =& \frac{1}{2}\left[\Pr\left\{|\mathbf{s}_u^H \mathbf{y}_u|^2 \leq \bar{z}_i, |\mathbf{s}_d^H \mathbf{y}_u|^2 \leq \bar{z}_i\right\} + \Pr\left\{|\mathbf{s}_u^H \mathbf{y}_d|^2 \leq \bar{z}_i, |\mathbf{s}_d^H \mathbf{y}_d|^2 \leq \bar{z}_i\right\}\right] \\ =& \Pr\left\{|\mathbf{s}_u^H \mathbf{y}_u|^2 \leq \bar{z}_i, |\mathbf{s}_d^H \mathbf{y}_u|^2 \leq \bar{z}_i\right\}. \end{aligned} \tag{24}$$

Define $\frac{\sigma_n^2}{2}\mathbf{s}_u^H \mathbf{s}_u \triangleq \mathbf{U}_1 \mathbf{\Lambda}_1 \mathbf{U}_1^H$ and $\frac{\sigma_n^2}{2}\mathbf{s}_d^H \mathbf{s}_d \triangleq \mathbf{U}_2 \mathbf{\Lambda}_2 \mathbf{U}_2^H$, where $\mathbf{U}_1$ and $\mathbf{U}_2$ are unitary matrices and $\mathbf{\Lambda}_1$ and $\mathbf{\Lambda}_2$ are diagonal matrices, and $\mathbf{b}_u = \frac{\sqrt{2}}{\sigma_n}\alpha_t \mathbf{s}_u$. Both terms in the argument of probability in (24) depend on same random $\mathbf{y}_u$, i.e., same random $\mathbf{n}_i$. Since both $\mathbf{\Lambda}_1$ and $\mathbf{\Lambda}_2$ are rank-one, and without loss of generality, we arrange $\mathbf{\Lambda}_1$ in ascending order and $\mathbf{\Lambda}_2$ in descending order. This key idea allows us to make the terms in the argument of probability in (24) to be statistically independent. Thus, following similar steps as in Appendix-A, $F_{\bar{Z}_i}(\bar{z}_i)$ can be expressed as

$$\begin{aligned} F_{\bar{Z}_i}(\bar{z}_i) =& \Pr\Big\{\left(\bar{\mathbf{b}}_{1,i} + \bar{\mathbf{n}}_{1,i}\right)^H \mathbf{\Lambda}_1 \left(\bar{\mathbf{b}}_{1,i} + \bar{\mathbf{n}}_{1,i}\right) \leq \bar{z}_i, \\ & \left(\bar{\mathbf{b}}_{2,i} + \bar{\mathbf{n}}_{2,i}\right)^H \mathbf{\Lambda}_2 \left(\bar{\mathbf{b}}_{2,i} + \bar{\mathbf{n}}_{2,i}\right) \leq \bar{z}_i\Big\}, \end{aligned} \tag{25}$$

where $\bar{\mathbf{b}}_{1,i} = \mathbf{U}_1^H \mathbf{b}_u$, $\bar{\mathbf{n}}_{1,i} = \mathbf{U}_1^H \bar{\mathbf{n}}_i$, $\bar{\mathbf{b}}_{2,i} = \mathbf{U}_2^H \mathbf{b}_u$, $\bar{\mathbf{n}}_{2,i} = \mathbf{U}_2^H \bar{\mathbf{n}}_i$, and $\bar{\mathbf{n}}_i = \frac{\sqrt{2}}{\sigma_n}\mathbf{n}_i$ such that each element of $\bar{\mathbf{n}}_i$ is distributed as $\mathcal{N}_C(0,2)$. Therefore, $F_{\bar{Z}_i}(\bar{z}_i)$ is given by

$$\begin{aligned} F_{\bar{Z}_i}(\bar{z}_i) =& \Pr\left\{\mu_1|\tilde{b}_{1,i} + \tilde{n}_{1,i}|^2 \le \bar{z}_i, \mu_2|\tilde{b}_{2,i} + \tilde{n}_{2,i}|^2 \le \bar{z}_i\right\}, \\ =& \Pr\left\{\bar{X}_i \le \bar{z}_i, \bar{Y}_i \le \bar{z}_i\right\}, \end{aligned} \tag{26}$$

where $\mu_1 = \mathbf{\Lambda}_1(L_c, L_c)$, $\mu_2 = \mathbf{\Lambda}_2(1,1)$, $\tilde{b}_{1,i} = \bar{\mathbf{b}}_{1,i}(L_c)$, $\tilde{b}_{2,i} = \bar{\mathbf{b}}_{2,i}(1)$, $\tilde{n}_{1,i} = \bar{\mathbf{n}}_{1,i}(L_c)$, $\tilde{n}_{2,i} = \bar{\mathbf{n}}_{2,i}(1)$, $\bar{X}_i \triangleq \mu_1|\tilde{b}_{1,i} + \tilde{n}_{1,i}|^2$ and $\bar{Y}_i \triangleq \mu_2|\tilde{b}_{2,i} + \tilde{n}_{2,i}|^2$ are scaled independent non-central Chi-square distributed random variables with 2 degrees of freedom. The PDFs of $\bar{X}_i$ and $\bar{Y}_i$ are, respectively, given by

$$f_{\bar{X}_i}(\bar{x}_i) = \frac{1}{2\mu_1} e^{-\frac{\bar{x}_i + \mu_1\lambda_x}{2\mu_1}} I_0\left(\sqrt{\frac{\lambda_x}{\mu_1}\bar{x}_i}\right), \; f_{\bar{Y}_i}(\bar{y}_i) = \frac{1}{2\mu_1} e^{-\frac{\bar{y}_i + \mu_2\lambda_y}{2\mu_2}} I_0\left(\sqrt{\frac{\lambda_y}{\mu_2}\bar{y}_i}\right), \tag{27}$$

where $I_0(x)$ denotes the zeroth-order modified Bessel function of the first kind [42], $\lambda_x = |\tilde{b}_{1,i}|^2$ and $\lambda_y = |\tilde{b}_{2,i}|^2$. The PDF of $\bar{Z}_i = \max(\bar{X}_i, \bar{Y}_i)$ is given by

$$f_{\bar{Z}_i}(\bar{z}_i) = f_{\bar{X}_i}(\bar{z}_i) \int_0^{\bar{z}_i} f_{\bar{Y}_i}(\bar{y}_i)\, d\bar{y}_i + f_{\bar{Y}_i}(\bar{z}_i) \int_0^{\bar{z}_i} f_{\bar{X}_i}(\bar{x}_i)\, d\bar{x}_i, \tag{28}$$

where

$$\begin{aligned} \int_0^{\bar{z}_i} f_{\bar{Y}_i}(\bar{y}_i)\, d\bar{y}_i =& 1 - Q_1\left(\sqrt{\lambda_y}, \sqrt{\frac{\bar{z}_i}{\mu_2}}\right), \\ \int_0^{\bar{z}_i} f_{\bar{X}_i}(\bar{x}_i)\, d\bar{x}_i =& 1 - Q_1\left(\sqrt{\lambda_x}, \sqrt{\frac{\bar{z}_i}{\mu_1}}\right). \end{aligned} \tag{29}$$

Here, $Q_1(a,b)$ denotes Marcum-q function [42] of the first-order with the parameters a and b. Since the PDF of $\bar{Z}_i$ is already in complicated form, the PDF of $\bar{Z} = \sum_{i=1}^{L} \bar{Z}_i$ cannot be obtained in a closed-form. Toward this end, we apply Central Limit Theorem (CLT), which allows us to approximate $\bar{Z}$ as Gaussian distributed with mean $\mu_{\bar{Z}}$ and variance $\sigma_{\bar{Z}}^2$. □

Proposition 3 *The approximated detection probability in terms of Gaussian Q-function can be given by*

$$\bar{P}_D \approx Q\left(\frac{\gamma_{\text{th}} - \mu_{\bar{Z}}}{\sigma_{\bar{Z}}}\right). \tag{30}$$

1 ***Proof***

Refer to Appendix C.

The accuracy of this approximation will be examined with simulations for different parameter settings. □

4 Ambiguity function of up- and down- chirps

Target detection and resolvability depends on whether the given radar waveform satisfies desired requirements in terms of CAF, which is a function of delay and Doppler. Below, we analyze the CAF where the data comprises of a sequence of up- and down-chirps. With N-chirp sequence, we have

$$x(t) = \frac{1}{\sqrt{T}} \sum_{k=0}^{N-1} \text{rect}\left(\frac{t - kT_p - \frac{T}{2}}{T}\right) e^{j(2\pi f_0 t + q_k \pi \alpha t^2)} \tag{31}$$

where q_k takes value 1 for up-chirp and -1 for down-chirp, and T_p is the PRI of the chirp waveform. The two-dimensional CAF can be defined as

$$X(\tau; f_d) = \int_{-\infty}^{\infty} x(t) x^*(t-\tau) e^{j2\pi f_d t} dt, \tag{32}$$

where τ and f_d, respectively, denote delay and Doppler domains. Using (31) and (32) and skipping the carrier frequency part, for the sake of conciseness, the CAF can be expressed as

$$\begin{aligned} X(\tau; f_d) =& \frac{1}{T} \sum_{k=0}^{N-1} \sum_{l=0}^{N-1} \int_{-\infty}^{\infty} \left\{ \text{rect}\left(\frac{t - kT_p - \frac{T}{2}}{T}\right) \text{rect}\left(\frac{t - \tau - lT_p - \frac{T}{2}}{T}\right) \times \right. \\ & \left. e^{jq_k \pi \alpha (t - kT_p)^2} e^{-jq_l \pi \alpha (t - lT_p - \tau)^2} e^{j2\pi f_d t} dt \right\}, \\ =& \frac{1}{T} \sum_{k=0}^{N-1} \sum_{l=0}^{N-1} e^{j\pi \alpha \bar{\tau}_{k,l}} \int_{-\infty}^{\infty} p_{k,l}(t) e^{jq_{k,l} \pi \alpha t^2} e^{j2\pi \beta_{k,l} t} dt, \end{aligned} \tag{33}$$

where we use $\bar{\tau}_{k,l} \triangleq q_k k^2 T_p^2 - q_l (lT_p + \tau)^2$, $\beta_{k,l} \triangleq \alpha\left(q_l (lT_p + \tau) - q_k kT_p\right) + f_d$, $p_{k,l}(t) \triangleq \text{rect}\left(\frac{t - kT_p - \frac{T}{2}}{T}\right) \text{rect}\left(\frac{t - \tau - lT_p - \frac{T}{2}}{T}\right)$, and $q_{k,l} = q_k - q_l$ for notational convenience. Using the definition of rectangular function, we can express $p_{k,l}(t)$ as

$$p_{k.l}(t) = \begin{cases} 1 \text{ if } lT_p + \tau \le t \le kT_p + T, \ (k-l)T_p \le \tau \le (k-l)T_p + T \\ 1 \text{ if } kT_p \le t \le lT_p + \tau + T, \ (k-l)T_p - T \le \tau \le (k-l)T_p \\ 0 \qquad\qquad\qquad\qquad \text{otherwise} \end{cases} \tag{34}$$

Let the two regions of τ in (34) be represented as $\mathcal{R}_1 \triangleq (k-l)T_p \le \tau \le (k-l)T_p + T$ and $\mathcal{R}_2 \triangleq (k-l)T_p - T \le \tau \le (k-l)T_p$.

Proposition 4 *The CAF $X(\tau; f_d)$ for a sequence of N up- and down- chirps can be expressed as*

$$X(\tau; f_d) = \begin{cases} X_1(\tau; f_d) + X_2(\tau; f_d) & \text{if } \tau \in \mathcal{R}_1 \\ \bar{X}_1(\tau; f_d) + \bar{X}_2(\tau; f_d) & \text{if } \tau \in \mathcal{R}_2 \end{cases} \tag{35}$$

where $X_1(\tau; f_d)$, $X_2(\tau; f_d)$, $\bar{X}_1(\tau; f_d)$, $\bar{X}_2(\tau; f_d)$ are derived in Appendix D.

Note that $X_1(\tau; f_d)$ and $\bar{X}_1(\tau; f_d)$ correspond to those terms of the CAF for which $q_{k,l} = 0, \forall k, l$, whereas $X_2(\tau; f_d)$ and $\bar{X}_2(\tau; f_d)$ correspond to the terms for which

$q_{k,l} = \pm 2$. In the case of only up- (or down-) chirps, all terms of the CAF correspond to $q_{k,l} = 0, \forall k, l$, meaning that the CAF does not include $X_2(\tau; f_d)$ and $\bar{X}_2(\tau; f_d)$.

5 Waveform diversity with OCDM

The data transmission rate of up- and down- chirps can be improved by employing orthogonal chirp waveforms. It was shown in [43] that OCDM outperforms orthogonal frequency division multiplexing (OFDM), in terms of BER for different modulation orders and linear receivers, under frequency selective fading channels in single-input single-output case. The viability of OCDM in a MIMO case with different space time coding techniques was investigated in [44], which also showed that OCDM outperforms OFDM in terms of frame error rate. Although OCDM is favored in communications systems, to the best of the authors' knowledge, there has been no investigation in the literature in determining the suitability of OCDM for radar operation and functionality. For this purpose, we will derive the CAF of OCDM waveform. Under the framework of Fresnel transform, the set of N-orthogonal chirps can be defined as

$$\Psi_k(t) = \frac{1}{\sqrt{T}}\text{rect}\left(\frac{t}{T}\right)\Phi_a\left(t - \frac{kT}{N}\right) = \frac{1}{\sqrt{T}}\mathrm{e}^{\frac{j\pi}{4}}\mathrm{e}^{\frac{-j\pi}{a}\left(t-\frac{kT}{N}\right)^2},\ 0 \le t \le T, \tag{36}$$

where $\Phi_a(t) = \frac{1}{\sqrt{T}}\mathrm{e}^{\frac{j\pi}{4}}\mathrm{e}^{\frac{-j\pi}{a}t^2}$, $a = \frac{T^2}{N}$, $k = 0, \ldots, N-1$, and the time-bandwidth product is given by $BT = N$. It can be shown that the above chirps are orthogonal, i.e.,

$$r_\Psi = \int_0^T \Psi_k(t)\Psi_m^*(t)\,dt = Te^{j\pi(k-m)}\text{sinc}(k-m), \tag{37}$$

where, the sinc-function, $\text{sinc}(k-m)$, is zero for all values of $k \neq m$ and 1 for $k = m$. Each orthogonal chirp is modulated with information carrying symbol drawn randomly from a digital modulation constellation. Let $\{s_k\}_{k=0}^{N-1} \in \mathcal{S}$ be symbols from the constellation $\mathcal{S}$. The transmitted OCDM signal is then expressed as

$$x(t) = \sum_{k=0}^{N-1} s_k\Psi_k(t) = \sum_{k=0}^{N-1}\frac{1}{\sqrt{T}}\text{rect}\left(\frac{t}{T}\right)s_k\mathrm{e}^{\frac{j\pi}{4}}\mathrm{e}^{\frac{-j\pi}{a}\left(t-\frac{kT}{N}\right)^2}. \tag{38}$$

Substituting (38) into (32), the CAF for OCDM signal can be obtained.

Proposition 5 *The CAF of OCDM signal can be expressed as*

$$\begin{aligned} X(\tau; f_d) = &\left(1 - \frac{|\tau|}{T}\right)\sum_{k=0}^{N-1}\sum_{l=0}^{N-1}\left\{s_k s_l^*\mathrm{e}^{-\frac{j\pi}{B^2}(k^2-l^2)}\mathrm{e}^{\frac{j\pi\tau}{T}(k-l+2lB^2+f_dT)}\times\right. \\ &\left.\text{sinc}\left(\left(1-\frac{|\tau|}{T}\right)\left(k-l-\frac{N\tau}{T}+f_dT\right)\right)\right\}. \end{aligned} \tag{39}$$

1 ***Proof***

Refer to Appendix E.

For $\tau = 0$, we obtain the amplitude of the zero-delay cut of the CAF as

$$\begin{aligned}|X(0;f_d)| &= \left|\sum_{k=0}^{N-1}\sum_{l=0}^{N-1} s_k s_l^* \mathrm{e}^{-\frac{j\pi}{B^2}(k^2-l^2)}\mathrm{sinc}\big((k-l+f_dT)\big)\right|,\\ &= \left|\sum_{k=0}^{N-1}|s_k|^2\mathrm{sinc}(f_dT) + \sum_{k=0}^{N-1}\sum_{l\neq k,l=0}^{N-1} s_k s_l^* \mathrm{e}^{-\frac{j\pi}{B^2}(k^2-l^2)}\frac{(-1)^{k-l}\mathrm{sinc}(f_dT)}{\left[1+\frac{(k-l)}{f_dT}\right]}\right|.\end{aligned} \tag{40}$$

Similarly, the amplitude of the zero-Doppler cut of the CAF is given by

$$\begin{aligned}|X(\tau;0)| &= \left|\left(1-\frac{|\tau|}{T}\right)\sum_{k=0}^{N-1}\sum_{l=0}^{N-1} s_k s_l^* \mathrm{e}^{-\frac{j\pi}{B^2}(k^2-l^2)}\mathrm{e}^{j\frac{\pi\tau}{T}(k-l+2lB^2)}\mathrm{sinc}\left(\left(k-l+\frac{N\tau}{T}\right)\right)\right|,\\ &= \left|1-\frac{|\tau|}{T}\right|\left|\sum_{k=0}^{N-1}|s_k|^2\mathrm{e}^{j\frac{\pi\tau}{T}k(2B^2)}\mathrm{sinc}(B\tau) + \sum_{k=0}^{N-1}\sum_{l\neq k,l=0}^{N-1} s_k s_l^* \mathrm{e}^{-\frac{j\pi}{B^2}(k^2-l^2)}\times\right.\\ &\quad \left.\mathrm{e}^{j\frac{\pi\tau}{T}(k-l+2lB^2)}\frac{(-1)^{(k-l)}\mathrm{sinc}(B\tau)}{\left[1+\frac{k-l}{B\tau}\right]}\right|.\end{aligned} \tag{41}$$

Note that the CAF (39) as well as its specific cases given by (40) and (41) revert to standard ambiguity function of a chirp waveform when $N = 1$. The mainlobe widths and PSR of both zero-Doppler and zero-delay cuts will be examined with computer simulations in the following section. □

6 Results and discussions

For all simulations, the required PFA is set to 10^{-3}. The noise power is set to 0 dBW, whereas α_t, which includes transmit power, transmit and receive antenna gains, target ranges, and RCS, is varied to change the SNR $\triangleq \frac{\alpha_t}{\sigma_n^2}$. While calculating the bit error probability in (13), we verified that taking 30 terms for each l and k are sufficient to confirm the convergence of the infinite series.

The simulated and theoretical bit error probabilities versus SNR are shown in Fig. 3 for different values of B and T. The sampling frequency, f_s, is chosen as 300 MHz, so that $L_c = f_sT$ turns out to be 300 for Fig. 3a and 60 for Fig. 3b. These figures show that the simulated and theoretical results exhibit very good matching, which validate the accuracy of the derived theoretical expression. Each figure shows that when B increases for a given T, the bit error probability decreases. Similarly, by comparing the two figures, we find that, for a given B, the bit error probability decreases when T increases. This improvement becomes more significant when increasing T from 0.2 to 1 μs for the bandwidth of 10 MHz than for 100 MHz. The reason is that $|\beta|$ decreases (as seen from (3)) when the time-bandwidth product of the chirp, BT, increases. When $|\beta|$ decreases, isolation (or decorrelation) between up- and down- chirps increases, which assists the receiver in discriminating between two chirps in the received signal.

The PFA versus threshold value in dB is shown in Fig. 4 for different values of L. As L increases, the PFA also increases. These curves give the threshold values for a given

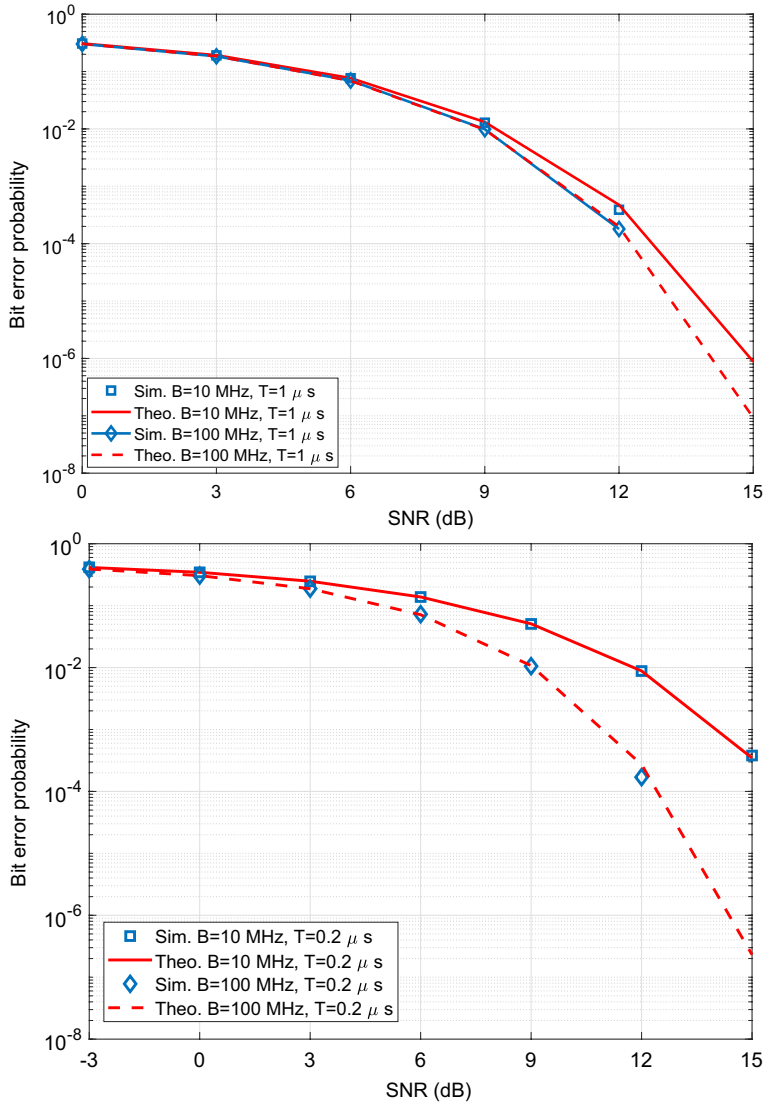

Fig. 3 Bit error probability versus SNR for different B and T: a-(top)) $L_c = 300$, b-(bottom)) $L_c = 60$

PFA. We can observe very good agreement between the simulated and theoretical PFA curves, which also verifies the correctness of the derived PFA expression.

In Fig. 5a, the simulated and theoretical (approximated) detection probabilities versus SNR are shown for different values of L. We chose $B = 10$ MHz, $T = 1\ \mu$s, and sampling frequency of $f_s = 300$ MHz so that $L_c = 300$. It can be observed from this figure that the detection probability increases as L increases. This shows that, by integrating target reflected signals from L pulses carrying different information (chirps), the performance of the radar system will not be compromised. Moreover, the maximum difference between the approximated and simulated detection probabilities is limited to approximately 0.1.

The theoretical and simulated detection probabilities as a function of SNR are shown in Fig. 5b for different B and T, and fixed $L = 100$. The theoretical and simulated results show very good matching when time-bandwidth product is high. This figure also

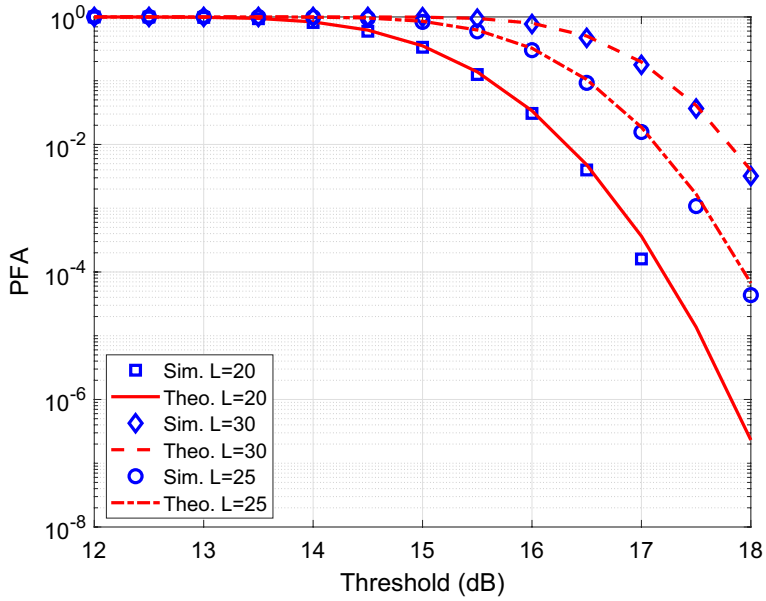

Fig. 4 PFA versus threshold value for different L

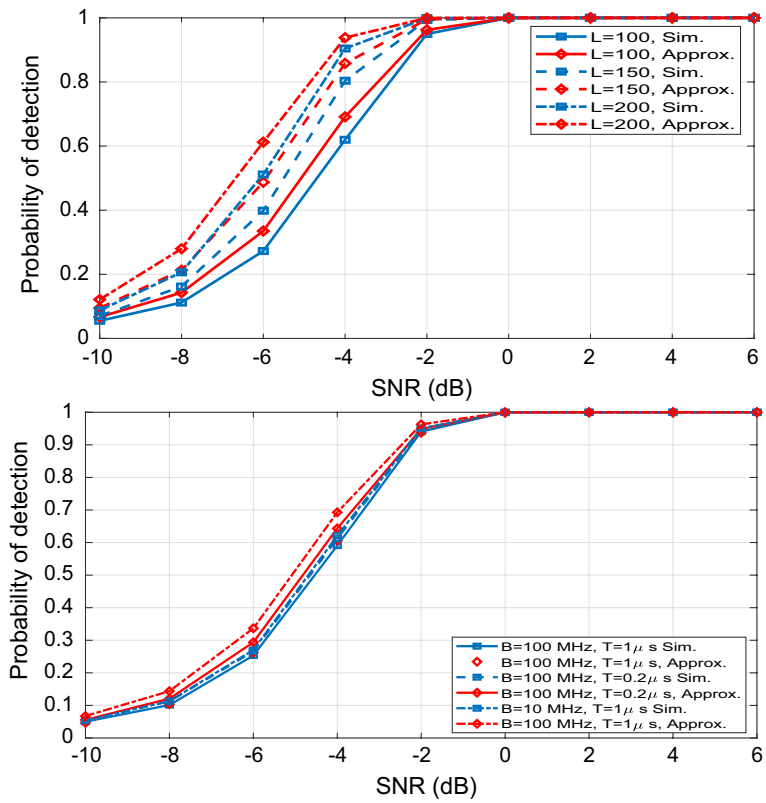

Fig. 5 Probability of detection versus SNR for a-(top)) different *L*, b-(bottom)) different time-bandwidth product

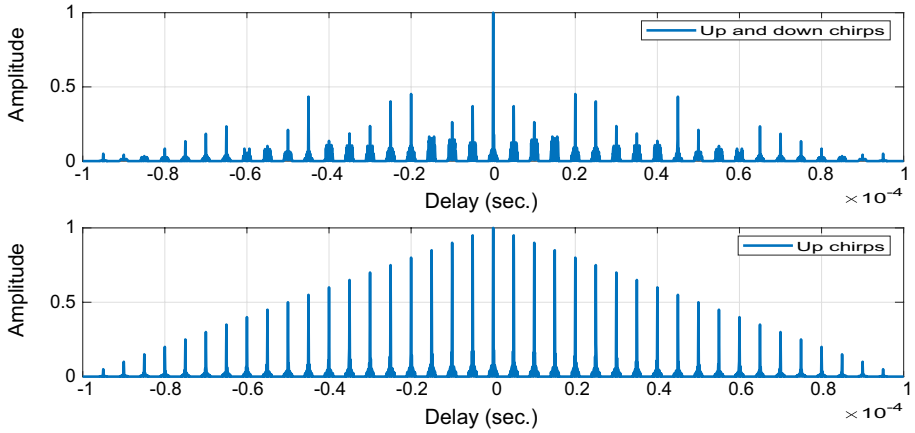

Fig. 6 Zero-Doppler cut of the CAF for a sequence of a-(top)) up- and down- chirps, b-(bottom)) only up-chirps

shows that the detection performance slightly improves when time-bandwidth product decreases, which causes less signal isolation, i.e., both matched filter output will indicate higher probability of target presence in the reflected signal. This result is worth noting since the bit error rate improves when time-bandwidth product increases, due to an increase in signal isolation. Accordingly, higher signal isolation is good for performance in terms of bit error rate, but bad for detection performance.

6.1 CAF of up- and down- chirps

In this subsection, we will present results to demonstrate how transmitting random information bits with up- and down- chirps can improve zero-Doppler cut of the CAF, while keeping zero-Delay cut similar to that in the case with all up- or down- chirp transmission. For this purpose, we select following chirp parameters: pulse width of 1 μs, PRI of 5 μs, bandwidth (B) of 10 MHz, and sampling frequency of 300 MHz.

Figure 6 shows zero-Doppler cuts of the CAF when using up- and down- chirps and only up- (or down-) chirps. In the former case, 20 bits of random information are transmitted with $N = 20$ chirp waveforms, whereas in the latter case, 20 bits but all 1s are transmitted with $N = 20$ chirp waveforms. In both cases, the CAF replicas repeat at delays equal to the integer multiples of the PRI. Within each replica, the first null or the first lowest value of the CAF amplitude occurs at a distance of $\frac{1}{B}$ from the center of the replica. However, compared to the case with only up- (or down-) chirps, as shown at the bottom of Fig. 6, the amplitudes of the replicas decrease as τ increases in the case of using both up- and down- chirps. This shows that, compared to only up- (or down-) chirp transmission, the proposed transmission of random information bits with up- and down- chirps is helpful in decreasing the range sidelobe levels significantly. This improvement can be explained as follows. In (35), the CAF is a summation of two parts, where the first part is due to up- (or down-) chirps, whereas the second part is due to alternating transmission of up- and down- chirps. When random information bits are transmitted, if two consecutive bits alternate between 0 and 1, the second part of the CAF decreases and the number of summation terms in the first part decreases, thereby decreasing the range sidelobe amplitudes of the CAF.

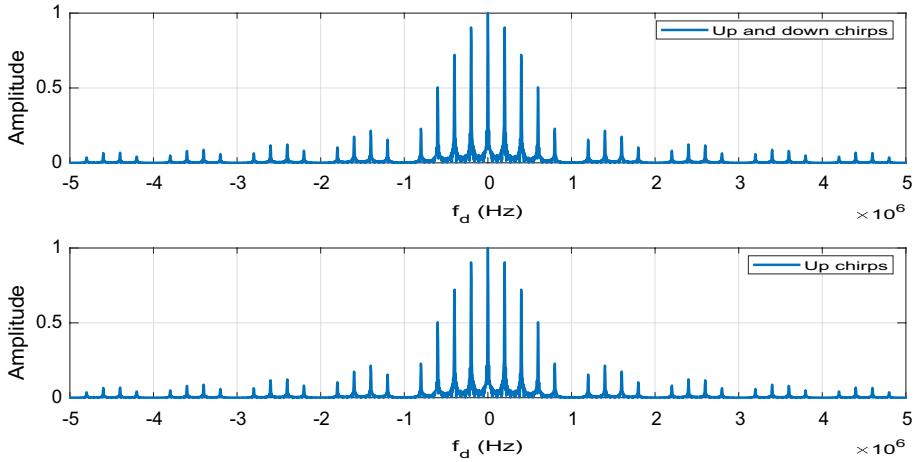

Fig. 7 Zero-delay cut of the CAF for a sequence of a-(top)) up- and down- chirps, b-(bottom)) only up-chirps

In Fig. 7, we show zero-delay cuts of the CAF when using up- and down- chirps and only up- (or down-) chirps. In contrast to the gain obtained in terms of decreased sidelobe levels in the zero-Doppler cuts of the CAF in Fig. 7, the proposed up- and down- chirp transmission does not provide additional gains over the zero-Doppler cuts of the CAF obtained with only up- (or down-) chirp transmission.

6.2 OCDM results

The performance improvement of OCDM over OFDM, in terms of bit error rate, has been already demonstrated in [43]. In this subsection, we show numerical results for delineating the advantages of OCDM over standard chirp-based radar sensing. For this purpose, we fix the bandwidth of OCDM to 10 MHz and plot the amplitudes of the zero-Doppler and zero-delay cuts of the CAF for different numbers of orthogonal chirps, N. Since the time-bandwidth product is $BT = N$, T increases when N increases. The orthogonal chirps carry random QPSK modulated symbols.

The zero-Doppler cut of the CAF, $|X(\tau, 0)|$ (41), is shown in Fig. 8a for different values of N. Although the single chirp case shows multiple deep nulls in sidelobes, the amplitudes of several sidelobes (first to fourth) adjacent to the mainlobe decrease when N increases. Moreover, although the two ends of the mainlobe do not exhibit deeper nulls as in the case of $N = 1$, the main sidelobe width remains comparable or smaller to $N = 1$ (which is $T = \frac{N}{B} = B$), when N increases. These results indicate that OCDM can improve radar performance in terms of target range estimation. In Fig. 8b, we show amplitude of the zero-delay cut of the CAF (40) for different N. When N increases, the mainlobe width decreases by a factor of N, i.e., from $f_d = \frac{1}{T} = B$ in single chirp case to $f_d = \frac{1}{T} = \frac{B}{N}$ in N orthogonal chirps case. In addition, the sidelobe levels are comparable to or smaller than in the case with $N = 1$. From these results, we observe that OCDM provides better Doppler resolution capabilities than single chirp-based modulation. Based on the relation, $BT = N$, the mainlobe width of the zero-Doppler cut should increase proportionally with N and that of the zero-delay cut should decrease proportionally with N. OCDM maintains the latter good property which is important

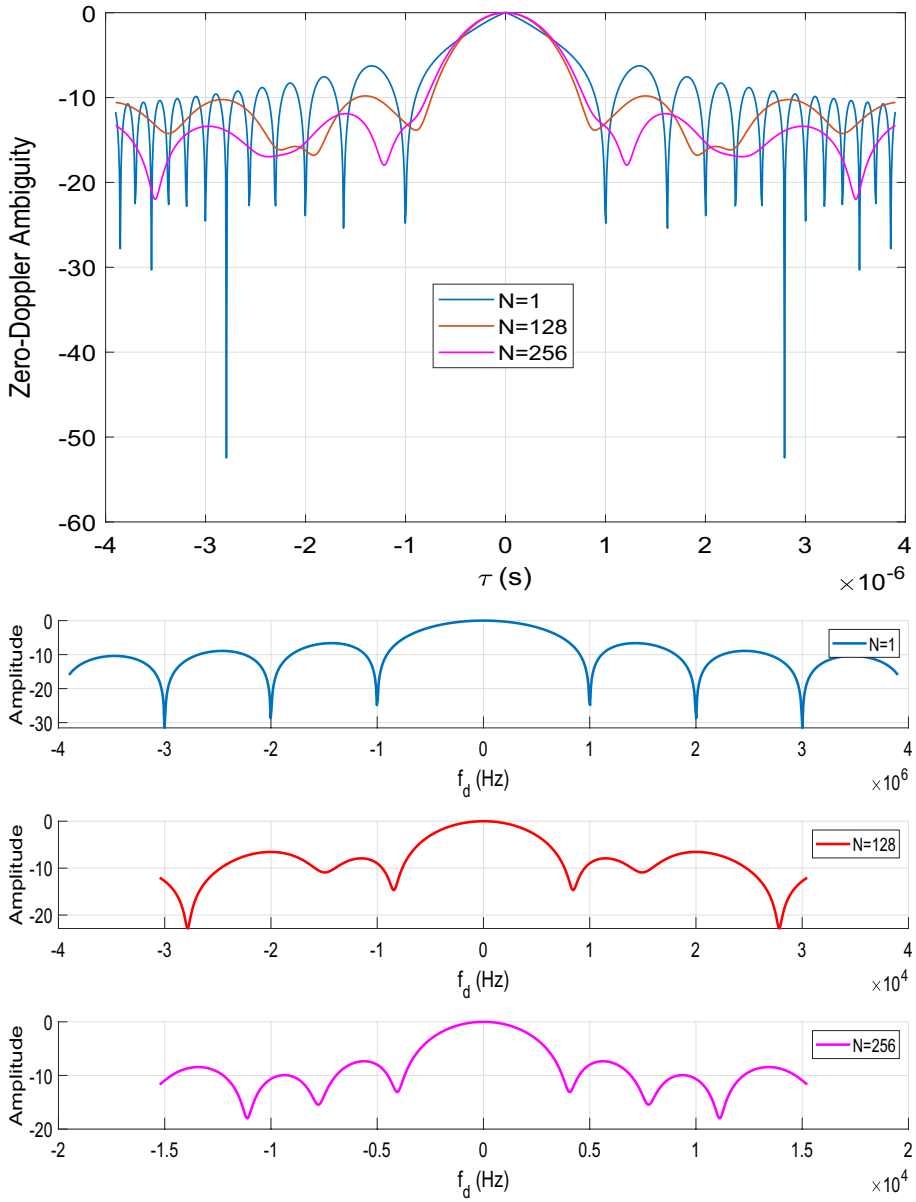

Fig. 8 Amplitude of the OCDM CAF: a-(top)) zero-Doppler cut, b-(bottom)) zero-delay cut

for enhancing Doppler estimation and resolution. On the other hand, OCDM does not allow the mainlobe width of the zero-Doppler cut to increase beyond B.

7 Conclusions

We proposed approaches for embedding target information and scheduling data in radar waveforms, with the objective of improving radar functionality in a radar network. The performance analysis, for sharing scheduling data carried by up-and down-chirps, demonstrated that the bit error probability decreases with increased isolation between up- and down- chirps, which is achieved by increasing the time-bandwidth product. On the other hand, detection probability slightly decreased

with increasing the time-bandwidth product. By deriving cross-ambiguity function (CAF) of a sequence of up- and down- chirps, we showed its capability to decrease range sidelobe levels compared to the transmission of only up- (or down-) chirps. To improve the underlying data rate transmission of such a scheme, we proposed orthogonal chirp division multiplexing (OCDM) for dual function radar systems. Our analysis on the CAF shows that the OCDM provides improved sensing performance as seen from the mainlobe widths and the sidelobe levels of the zero-Doppler and zero-delay cuts. The proposed chirp-based waveform diversity approach and its performance analysis will be extended to the cluttered environments in future work.

Appendix A: Proof of Proposition 1

The probability of bit error of (9) can be expressed as

$$\begin{aligned} P_b =& \Pr\left\{ \mathbf{y}_u^H \underbrace{\left[\mathbf{s}_u\mathbf{s}_u^H - \mathbf{s}_d\mathbf{s}_d^H\right]}_{\mathbf{A}} \mathbf{y}_u \le 0 \right\}, \\ =& \Pr\left\{ (\mathbf{n} + \alpha_t \mathbf{s}_u)^H \mathbf{A} (\mathbf{n} + \alpha_t \mathbf{s}_u) \le 0 \right\}, \\ =& \Pr\left\{ (\sigma_n \bar{\mathbf{n}} + \mathbf{b})^H \mathbf{A} (\sigma_n \bar{\mathbf{n}} + \mathbf{b}) \le 0 \right\}, \\ =& \Pr\left\{ \left(\bar{\mathbf{n}} + \mathbf{b}\sigma_n^{-1}\right)^H \bar{\mathbf{A}} \left(\bar{\mathbf{n}} + \mathbf{b}\sigma_n^{-1}\right) \le 0 \right\}, \end{aligned} \tag{42}$$

where $\mathbf{b} = \alpha_t \mathbf{s}_u$, $\bar{\mathbf{n}} = \frac{\mathbf{n}}{\sigma_n} \sim \mathcal{N}_C(0,1)$, and $\bar{\mathbf{A}} = \sigma_n^2 \mathbf{A}$. Let $\bar{\mathbf{b}} = \mathbf{b}\sigma_n^{-1}$ and eigenvalue decomposition of $\bar{\mathbf{A}}$ be given by $\bar{\mathbf{A}} = \mathbf{U}\mathbf{\Lambda}\mathbf{U}^H$, where $\mathbf{U}$ is the matrix of eigenvectors and $\mathbf{\Lambda}$ is the diagonal matrix of eigenvalues. Then, (42) can be expressed as

$$\begin{aligned} P_b =& \Pr\left\{ \left(\bar{\mathbf{n}} + \bar{\mathbf{b}}\right)^H \mathbf{U}\mathbf{\Lambda}\mathbf{U}^H \left(\bar{\mathbf{n}} + \bar{\mathbf{b}}\right) \le 0 \right\} \\ =& \Pr\left\{ \left(\mathbf{U}^H\bar{\mathbf{n}} + \mathbf{U}^H\bar{\mathbf{b}}\right)^H \mathbf{\Lambda} \left(\mathbf{U}^H\bar{\mathbf{n}} + \mathbf{U}^H\bar{\mathbf{b}}\right) \le 0 \right\}, \\ =& \Pr\left\{ \left(\tilde{\mathbf{n}} + \tilde{\mathbf{b}}\right)^H \mathbf{\Lambda} \left(\tilde{\mathbf{n}} + \tilde{\mathbf{b}}\right) \le 0 \right\}, \end{aligned} \tag{43}$$

where $\tilde{\mathbf{n}} = \mathbf{U}^H\bar{\mathbf{n}}$ and $\tilde{\mathbf{b}} = \mathbf{U}^H\bar{\mathbf{b}}$. Note that the elements of $\tilde{\mathbf{n}}$ remain zero-mean complex Gaussian distributed with unit variance as those of $\bar{\mathbf{n}}$ due to the fact that the statistics of Gaussian random vector is invariant to pre-/post-multiplication by a unitary matrix. Moreover, since $\bar{\mathbf{A}}$ is the difference between two rank-one matrices, it can be readily shown that the matrix $\bar{\mathbf{A}}$ has two non-zero (one positive and another negative) eigenvalues and remaining zero eigenvalues. Let these eigenvalues be denoted by λ_1 and λ_2, where $\lambda_1 > 0$ and $\lambda_2 < 0$. Note that these eigenvalues can be determined also in closed-form [45]. Without loss of generality, $\mathbf{\Lambda}$ can be expressed as $\mathbf{\Lambda} = \mathrm{diag}([\lambda_1, \lambda_2, 0, \ldots, 0])$. Thus, (43) can be expressed as

$$P_b = \Pr\left\{ \lambda_1 |\tilde{n}_1 + \tilde{b}_1|^2 \le |\lambda_2| |\tilde{n}_2 + \tilde{b}_2|^2 \right\}, \tag{44}$$

where $\tilde{n}_k$ and $\tilde{b}_k$ denote the k-th elements of $\tilde{\mathbf{n}}$ and $\tilde{\mathbf{b}}$, respectively. Since $\lambda_1 = |\lambda_2|$, which is due to $||\mathbf{s}_u||^2 = ||\mathbf{s}_d||^2$, we obtain the final expression (10).

Appendix B: Proof of Proposition 2

The PDF of the random variable $Z_i \triangleq \max(X_i, Y_i)$ is given by

$$f_{Z_i}(z_i) = f_{X_i}(z_i)F_{Y_i}(z_i) + F_{X_i}(z_i)f_{Y_i}(z_i) = e^{-\frac{z_i}{2}} - e^{-z_i}, \tag{45}$$

where $F_{Y_i}(z_i) = \int_0^{z_i} f_{Y_i}(x)\,dx$ and $F_{X_i}(z_i) = \int_0^{z_i} f_{X_i}(y)\,dy$. Let $Z = \sum_{i=1}^{L} Z_i$. To obtain the PDF of Z, we calculate the characteristic function, $\psi_Z(s) = \prod_{i=1}^{L} \psi_{Z_i}(s)$, of Z, where $\psi_{Z_i}(s)$ can be expressed as

$$\psi_{Z_i}(s) = \int_0^{\infty} e^{jsz_i} f_{Z_i}(z_i)\,dz_i = \frac{1}{(1-js)(1-2js)}. \tag{46}$$

Thus, the characteristic function of Z is $\psi_Z(s) = \prod_{i=1}^{L} \frac{1}{(1-js)(1-2js)}$. Consequently, the PDF of Z is obtained from $\psi_Z(s)$ as

$$f_Z(z) = \frac{1}{2\pi}\int_{-\infty}^{\infty} \psi_Z(s)e^{-jsz}\,ds = \frac{1}{2^L 2\pi}\int_{-\infty}^{\infty} (1-jt)^{-L}\left(\frac{1}{2}-jt\right)^{-L} e^{-jsz}\,ds. \tag{47}$$

Applying [eq. 3.384.7.6 [42]], (47) can be expressed as

$$f_Z(z) = \frac{e^{-\frac{z}{2}} z^{2L-1}}{2^L\Gamma(2L)}\,{}_1F_1\left(L; 2L; -\frac{1}{2}z\right), \tag{48}$$

where $\Gamma(\cdot)$ denotes complete Gamma function and ${}_1F_1(a; b; x)$ denotes confluent hypergeometric function [42]. Utilizing the derived PDF, the PFA of (20) is expressed as

$$P_f = 1 - \int_0^{\frac{2\gamma_{\text{th}}}{\sigma_n^2}} \frac{e^{\frac{-z}{2}} z^{2L-1}}{2^L\Gamma(2L)}\,{}_1F_1\left(L; 2L; \frac{-z}{2}\right) dz. \tag{49}$$

The integral (49) does not have a closed-form solution. Substituting following integral for ${}_1F_1\left(L; 2L; \frac{-z}{2}\right)$ [46]

$${}_1F_1\left(L; 2L; \frac{-z}{2}\right) = \frac{\Gamma(2L)}{(\Gamma(L))^2}\int_0^1 e^{-\frac{uz}{2}} u^{(L-1)}(1-u)^{L-1}\,du, \tag{50}$$

into (49) and then interchanging the integration order, we obtain

$$P_f = 1 - \frac{1}{2^L(\Gamma(L))^2}\int_0^1 u^{L-1}(1-u)^{L-1}\left[\int_0^{\frac{2\gamma_{\text{th}}}{\sigma_n^2}} e^{-\frac{(1+u)z}{2}} z^{2L-1}\,dz\right] du. \tag{51}$$

Applying [3.381.1, [42]] to inner integral in (51), we have

$$P_f = 1 - \frac{1}{2^{-L}(\Gamma(L))^2}\int_0^1 u^{L-1}(1-u)^{L-1}(1+u)^{-2L}\gamma\left(2L, \frac{(1+u)\gamma_{\text{th}}}{\sigma_n^2}\right) du, \tag{52}$$

where $\gamma(n+1,x)$ denotes lower incomplete Gamma function. Substituting its series form [8.352.1 [42]] into (52), we can express P_f as

$$\begin{aligned} P_f =& 1 - \frac{(2L-1)!}{2^{-L}(\Gamma(L))^2}\Bigg\{\int_0^1 u^{L-1}(1-u)^{L-1}(1+u)^{-2L} \\ &\times\left[1 - e^{-\frac{\gamma_{\text{th}}(1+u)}{\sigma_n^2}}\sum_{m=0}^{2L-1}\frac{\gamma_{\text{th}}^m(1+u)^m}{m!\sigma_n^{2m}}\right]du\Bigg\}, \\ =& 1 - \frac{(2L-1)!}{2^{-L}(\Gamma(L))^2}\left(J_1 - e^{-\frac{\gamma_{\text{th}}}{\sigma_n^2}}\sum_{m=0}^{2L-1}\frac{\gamma_{\text{th}}^m}{m!\sigma_n^{2m}}J_{2,m}\right), \end{aligned} \tag{53}$$

where

$$\begin{aligned} J_1 &= \int_0^1 \frac{u^{L-1}(1-u)^{L-1}}{(1+u)^{2L}}\,du, \\ J_{2,m} &= \int_0^1 u^{L-1}(1-u)^{L-1}(1+u)^{m-2L}e^{-\frac{\gamma_{\text{th}}u}{\sigma_n^2}}\,du. \end{aligned} \tag{54}$$

Applying [3.197.4 and 3.385 [42]], respectively, J_1 and $J_{2,m}$ can be expressed as

$$J_1 = 2^{-L}B(L,L),\; J_{2,m} = B(L,L)\Phi_1\left(L, 2L-m, 2L, \frac{-\gamma_{\text{th}}}{\sigma_n^2}, -1\right), \tag{55}$$

where $\Phi_1(\,)$ is the Gauss hypergeometric function of two variables [42]. With these derivations, the proof for **Proposition** 2 is completed.

Appendix C: Proof of Proposition 3

Note that $\mu_{\bar{Z}} = \sum_{i=1}^{L}\mathbb{E}\{\bar{Z}_i\}$, where $\mathbb{E}\{\bar{Z}_i\} = \int_0^\infty \bar{z}_i f_{\bar{Z}_i}(\bar{z}_i)$ is expressed as

$$\mathbb{E}\{\bar{Z}_i\} = \int_0^\infty \bar{z}_i f_{\bar{X}_i}(\bar{z}_i)\,d\bar{z}_i + \int_0^\infty \bar{z}_i f_{\bar{Y}_i}(\bar{z}_i)\,d\bar{z}_i - I_1 - I_2, \tag{56}$$

where

$$\begin{aligned} I_1 &= \int_0^\infty \bar{z}_i e^{-\frac{\bar{z}_i+\lambda_x\mu_1}{2\mu_1}} I_0\left(\sqrt{\lambda_x\frac{\bar{z}_i}{\mu_1}}\right) Q_1\left(\sqrt{\lambda_y}, \sqrt{\frac{\bar{z}_i}{\mu_2}}\right)d\bar{z}_i, \\ I_2 &= \int_0^\infty \bar{z}_i e^{-\frac{\bar{z}_i+\lambda_y\mu_2}{2\mu_2}} I_0\left(\sqrt{\lambda_y\frac{\bar{z}_i}{\mu_2}}\right) Q_1\left(\sqrt{\lambda_x}, \sqrt{\frac{\bar{z}_i}{\mu_1}}\right)d\bar{z}_i. \end{aligned} \tag{57}$$

Substituting the PDFs of $\bar{X}_i$ and $\bar{Y}_i$ from (27) into (56), we find that $\int_0^\infty \bar{z}_i f_{\bar{X}_i}(\bar{z}_i)\,d\bar{z}_i = \mu_1(\lambda_x+2)$ and $\int_0^\infty \bar{z}_i f_{\bar{Y}_i}(\bar{z}_i)\,d\bar{z}_i = \mu_2(\lambda_y+2)$. However, the closed form expressions for I_1 and I_2 cannot be obtained. After numerically calculating the integrals I_1 and I_2, the mean value of $\bar{Z}$ is expressed as

$$\mathbb{E}\{\bar{Z}\} = L\underbrace{\left[2(\mu_1+\mu_2) + \mu_1\lambda_x + \mu_2\lambda_y - I_1 - I_2\right]}_{\mathbb{E}\{\bar{Z}_i\}}. \tag{58}$$

On the other hand, the variance $\sigma_{\bar{Z}}^2$ can be expressed as $\sigma_{\bar{Z}}^2 = L\sigma_{\bar{Z}_i}^2$, where

$$\sigma_{\bar{Z}_i}^2 = \mathbb{E}\{\bar{Z}_i^2\} - [\mathbb{E}\{\bar{Z}_i\}]^2, \tag{59}$$

and

$$\mathbb{E}\{\bar{Z}_i^2\} = \int_0^\infty \bar{z}_i^2 f_{\bar{X}_i}(\bar{z}_i)\, d\bar{z}_i + \int_0^\infty \bar{z}_i^2 f_{\bar{Y}_i}(\bar{z}_i)\, d\bar{z}_i - I_3 - I_4, \tag{60}$$

with

$$\begin{aligned} I_3 &= \int_0^\infty \bar{z}_i^2 e^{-\frac{\bar{z}_i+\lambda_x\mu_1}{2\mu_1}} I_0\left(\sqrt{\lambda_x \frac{\bar{z}_i}{\mu_1}}\right) Q_1\left(\sqrt{\lambda_y}, \sqrt{\frac{\bar{z}_i}{\mu_2}}\right) d\bar{z}_i, \\ I_4 &= \int_0^\infty \bar{z}_i^2 e^{-\frac{\bar{z}_i+\lambda_y\mu_2}{2\mu_2}} I_0\left(\sqrt{\lambda_y \frac{\bar{z}_i}{\mu_2}}\right) Q_1\left(\sqrt{\lambda_x}, \sqrt{\frac{\bar{z}_i}{\mu_1}}\right) d\bar{z}_i. \end{aligned} \tag{61}$$

Using $f_{\bar{X}_i}(\bar{z}_i)$ and $f_{\bar{Y}_i}(\bar{z}_i)$ from (27) , we find that $\int_0^\infty \bar{z}_i^2 f_{\bar{X}_i}(\bar{z}_i)\, d\bar{z}_i = \mu_1^2((2+\lambda_x)^2 + 2(2+2\lambda_x))$ and $\int_0^\infty \bar{z}_i^2 f_{\bar{Y}_i}(\bar{z}_i)\, d\bar{z}_i = \mu_2^2((2+\lambda_y)^2 + 2(2+2\lambda_y))$. However, the integrals I_3 and I_4 have to be numerically evaluated. After finding the mean and variance of $\bar{Z}$, which is assumed to be Gaussian distributed, the probability of detection is finally expressed in terms of Gaussian Q-function as in (30) of **Proposition** 3.

Appendix D: Proof of Proposition 4

For $\mathcal{R}_1$, the CAF can be expressed as

$$X(\tau; f_d) = \frac{1}{T}\sum_{k=0}^{N-1}\sum_{l=0}^{N-1} e^{j\pi\alpha\bar{\tau}_{k,l}} \int_{lT_p+\tau}^{kT_p+T} e^{jq_{k,l}\pi\alpha t^2} e^{j2\pi\beta_{k,l}t}\, dt, \tag{62}$$

To the best of our knowledge, integral in (62) does not have a closed-form solution. However, considering that $q_{k,l}$ can only take values of 0, 2, and -2, we show that separate analytical expressions are tractable for these values.

Case 1 ($q_{k,l} = 0$): In this case, (62) can be expressed as

$$X_1(\tau; f_d) = \frac{1}{T}\sum_{k=0}^{N-1}\sum_{l=0}^{N-1} e^{j\pi\alpha\bar{\tau}_{k,l}} \int_{lT_p+\tau}^{kT_p+T} e^{j2\pi\beta_{k,l}t}\, dt, \tag{63}$$

After some straightforward derivations, we solve the integral in (63) and obtain

$$\begin{aligned} X_1(\tau; f_d) = \frac{1}{T}\sum_{k=0}^{N-1}\sum_{l=0}^{N-1} \Big\{ & e^{j\pi\alpha\bar{\tau}_{k,l}} e^{j\pi\beta_{k,l}((k+l)T_p+T+\tau)} \times \\ & ((k-l)T_p + T - \tau)\mathrm{sinc}\big(\beta_{k,l}((k-l)T_p + T - \tau)\big) \Big\}. \end{aligned} \tag{64}$$

Case 2 ($q_{k,l} = \pm 2$): In this case, after some simple manipulations of (62), we obtain

$$X_2(\tau;f_d) = \frac{1}{T}\sum_{k=0}^{N-1}\sum_{l=0}^{N-1} e^{j\pi\alpha\bar{\tau}_{k,l}} e^{\mp j\pi\frac{\beta_{k,l}^2}{2\alpha}} \int_{lT_p+\tau}^{kT_p+T} e^{\pm j2\pi\alpha\left(t\pm\frac{\beta_{k,l}}{2\alpha}\right)^2} dt. \tag{65}$$

Let the integral in (65) be denoted by $\bar{I}_1$ which can be expressed as

$$\bar{I}_1 = \int_{lT_p+\tau}^{kT_p+T} \cos\left(2\pi\alpha\left(t\pm\frac{\beta_{k,l}}{2\alpha}\right)^2\right)dt \pm j\int_{lT_p+\tau}^{kT_p+T} \sin\left(2\pi\alpha\left(t\pm\frac{\beta_{k,l}}{2\alpha}\right)^2\right)dt. \tag{66}$$

Substituting $t' = 2\sqrt{\alpha}\left(t\pm\frac{\beta_{k,l}}{2\alpha}\right)$ into (66), we obtain

$$\bar{I}_1 = \frac{1}{2\sqrt{\alpha}}\int_{u_1}^{u_2}\left[\cos\left(\frac{\pi}{2}t'^2\right)dt' \pm j\sin\left(\frac{\pi}{2}t'^2\right)\right]dt', \tag{67}$$

where u_1 and u_2 are defined as

$$u_1 = lT_p + \tau \pm \frac{\beta_{k,l}}{2\alpha},\ \ u_2 = kT_p + T \pm \frac{\beta_{k,l}}{2\alpha}. \tag{68}$$

Define $u_{\min} = \min(|u_1|,|u_2|)$ and $u_{\max} = \max(|u_1|,|u_2|)$. Then, $\bar{I}_1$ of (66) can be expressed as

$$\bar{I}_1 = \begin{cases} \frac{1}{2\sqrt{\alpha}}[(C(u_{\min}) - C(u_{\max})) \pm j(S(u_{\min}) - S(u_{\max}))] & \text{if } \frac{u_1}{u_2} \geq 0, u_1 \geq u_2 \\ \frac{1}{2\sqrt{\alpha}}[(C(u_{\max}) - C(u_{\min})) \pm j(S(u_{\max}) - S(u_{\min}))] & \text{if } \frac{u_1}{u_2} \geq 0, u_2 \geq u_1 \\ \frac{1}{2\sqrt{\alpha}}[(C(u_{\max}) + C(u_{\min})) \pm j(S(u_{\max}) + S(u_{\min}))] & \text{if } \frac{u_1}{u_2} \leq 0, u_2 \geq u_1 \\ \frac{1}{2\sqrt{\alpha}}[(-C(u_{\max}) - C(u_{\min})) \pm j(-S(u_{\max}) - S(u_{\min}))] & \text{if } \frac{u_1}{u_2} \leq 0, u_1 \geq u_2 \end{cases} \tag{69}$$

where $C(x)$ and $S(x)$ are, respectively, the cosine and sine Fresnel integrals defined as in (4). We can similarly derive CAF for the region $\mathcal{R}_2$. For **Case 1** ($q_{k,l} = 0$), the expression equivalent to (64) can be expressed as

$$\begin{aligned}\bar{X}_1(\tau;f_d) = \frac{1}{T}\sum_{k=0}^{N-1}\sum_{l=0}^{N-1}\Big\{ & e^{j\pi\alpha\bar{\tau}_{k,l}} e^{j\pi\beta_{k,l}((l+k)T_p+T+\tau)} \times \\ & ((l-k)T_p + T + \tau)\mathrm{sinc}\big(\beta_{k,l}((l-k)T_p + T + \tau)\big)\Big\}.\end{aligned} \tag{70}$$

For **Case 2** ($q_{k,l} = \pm 2$) and region $\mathcal{R}_2$, the expression equivalent to (65) can be expressed as

$$\bar{X}_2(\tau;f_d) = \frac{1}{T}\sum_{k=0}^{N-1}\sum_{l=0}^{N-1} e^{j\pi\alpha\bar{\tau}_{k,l}} e^{\mp j\pi\frac{\beta_{k,l}^2}{2\alpha}} \underbrace{\int_{kT_p}^{lT_p+\tau+T} e^{\pm j2\pi\alpha\left(t\pm\frac{\beta_{k,l}}{2\alpha}\right)^2} dt}_{\tilde{I}_1}, \tag{71}$$

where $\tilde{I}_1$ can be expressed as in (69), but with $u_{\min}$ and $u_{\max}$ replaced by $\bar{u}_{\min} = \min(|\bar{u}_1|,|\bar{u}_2|)$ and $\bar{u}_{\max} = \max(|\bar{u}_1|,|\bar{u}_2|)$, respectively, where

$$\bar{u}_1 = kT_p \pm \frac{\beta_{k,l}}{2\alpha}, \;\; \bar{u}_2 = lT_p + \tau + T \pm \frac{\beta_{k,l}}{2\alpha}. \tag{72}$$

We have derived $X_1(\tau; f_d)$, $X_2(\tau; f_d)$, $\bar{X}_1(\tau; f_d)$, and $\bar{X}_2(\tau; f_d)$ required for **Proposition** 4.

Appendix E: Proof of Proposition 5

Substituting (38) into (32), we obtain

$$\begin{aligned} X(\tau; f_d) &= \int_{-\infty}^{\infty} \frac{1}{T} p(t) \sum_{k=0}^{N-1} s_k e^{j\frac{\pi}{4}} e^{-j\frac{\pi N}{T^2}\left(t-\frac{kT}{N}\right)^2} \sum_{l=0}^{N-1} s_k^* e^{-j\frac{\pi}{4}} e^{j\frac{\pi N}{T^2}\left(t-\tau-\frac{lT}{N}\right)^2} e^{j2\pi f_d t}\, dt, \\ &= \frac{1}{T} \sum_{k=0}^{N-1}\sum_{l=0}^{N-1} s_k s_l^* \int_{-\infty}^{\infty} p(t) e^{-j\frac{\pi N}{T^2}\left(t-\frac{kT}{N}\right)^2} e^{j\frac{\pi N}{T^2}\left(t-\tau-\frac{lT}{N}\right)^2} e^{j2\pi f_d t}\, dt, \\ &= \frac{1}{T} \sum_{k=0}^{N-1}\sum_{l=0}^{N-1} s_k s_l^* e^{j\pi \nu_{k,l}(\tau)} \underbrace{\int_{-\infty}^{\infty} p(t) e^{j\frac{2\pi}{T}\left(k-l-\frac{N\tau}{T}+f_d T\right)t}\, dt}_{\bar{I}}, \end{aligned} \tag{73}$$

where $p(t) = \text{rect}\left(\frac{t}{T}\right)\text{rect}\left(\frac{t-\tau}{T}\right)$ and $\nu_{k,l}(\tau) = \frac{(l^2-k^2)T^2}{N^2} + \frac{2lN^2}{T^3}\tau + \frac{N}{T^2}\tau^2$. $p(t)$ can be expressed as

$$p(t) = \begin{cases} 1 & \text{if } \tau - \frac{T}{2} \le t \le \frac{T}{2}, 0 \le \tau \le \frac{T}{2} \\ 1 & \text{if } -\frac{T}{2} \le t \le -\tau + \frac{T}{2}, \frac{-T}{2} \le \tau \le 0 \\ 0 & \text{otherwise} \end{cases} \tag{74}$$

For $0 \le \tau \le \frac{T}{2}$, after some straightforward derivations, $\bar{I}$ can be calculated as

$$\bar{I} = \int_{\tau-\frac{T}{2}}^{\frac{T}{2}} e^{j\frac{2\pi}{T}\left(k-l-\frac{N\tau}{T}+f_d T\right)t}\, dt = T\left(1-\frac{\tau}{T}\right) e^{j\frac{\pi}{T}\bar{f}\tau} \text{sinc}\left(\pi\bar{f}\left(1-\frac{\tau}{T}\right)\right), \tag{75}$$

where $\bar{f} \triangleq \left(k-l-\frac{N\tau}{T}+f_d T\right)$. Similarly, for $-\frac{\tau}{2} \le \tau \le 0$, $\bar{I}$ can be also expressed as

$$\bar{I} = \int_{-\frac{T}{2}}^{\frac{T}{2}-\tau} e^{j\frac{2\pi}{T}\left(k-l-\frac{N\tau}{T}+f_d T\right)t}\, dt, = T\left(1-\frac{\tau}{T}\right) e^{-j\frac{\pi}{T}\bar{f}\tau} \text{sinc}\left(\pi\bar{f}\left(1-\frac{\tau}{T}\right)\right). \tag{76}$$

Consequently, for $\frac{-T}{2} \le \tau \le 0$, $\bar{I}$ can be combined in the following form

$$\bar{I} = T\left(1-\frac{|\tau|}{T}\right) e^{j\frac{\pi}{T}\bar{f}\tau} \text{sinc}\left(\pi\bar{f}\left(1-\frac{|\tau|}{T}\right)\right). \tag{77}$$

Substituting $\bar{I}$ from (77) into (73), the CAF is expressed as

$$\begin{aligned} X(\tau; f_d) = &\left(1-\frac{|\tau|}{T}\right) \sum_{k=0}^{N-1}\sum_{l=0}^{N-1} \left\{ s_k s_l^* e^{j\pi\nu_{k,l}(\tau)} e^{j\frac{\pi}{T}\left(k-l-\frac{N\tau}{T}+f_d T\right)\tau} \times \right. \\ &\left. \text{sinc}\left(\left(k-l-\frac{N\tau}{T}+f_d T\right)\left(1-\frac{|\tau|}{T}\right)\right)\right\}. \end{aligned} \tag{78}$$

Re-substituting $\nu_{k,l}(\tau)$ into (78), we obtain the expression in **Proposition** 5, assuming that $\frac{\tau}{T} << 1$ and $\tau^2 << 1$.

Abbreviations

BER	Bit error rate
BPSK	Binary phase shift keying
CAF	Cross-ambiguity function
CDF	Cumulative distribution function
CLT	Central limit theorem
CPI	Coherent pulse interval
CSCG	Circularly symmetric complex Gaussian
DFRC	Dual function radar and communications systems
MIMO	Multiple-input multiple-output
MF	Matched filtering
MS	Monostatic
OCDM	Orthogonal chirp division multiplexing
OFDM	Orthogonal frequency division multiplexing
PFA	Probability of false alarm
PRI	Pulse repetition interval
PSR	Peak-to-sidelobe ratio
QPSK	Quadrature phase shift keying
RCS	Radar cross section
SNR	Signal-to-noise ratio

Acknowledgements
Not applicable.

Author contributions
The first author contributed to the problem formulation, derivations, simulations, analysis of the results, and writing of the paper. The second author contributed to the development of high level concepts, discussions on the derivations and results, and paper writing. The third author provided insights on problem formulation and coordinated overall collaboration among authors. All authors read and approved the final manuscript.

Funding
Not applicable.

Availability of data and materials
Data sharing is not applicable to this article as no datasets were generated or analyzed during the current study.

Declarations

Ethics approval and consent to participate
This manuscript does not involve human participants, human data or human tissue.

Consent for publication
All authors agree to publish this manuscript.

Competing interests
The authors declare that they have no competing interests.

Received: 29 August 2022 Accepted: 20 December 2022
Published online: 26 January 2023

References

1. A.F. Martone, K. Ranney, K. Sherbondy, K.A. Gallagher, S.D. Blunt, Spectrum allocation for noncooperative radar coexistence. IEEE Trans. Aerosp. Electron. Syst. **54**(1), 90 (2018)
2. A. Martone, M. Amin, A view on radar and communication systems coexistence and dual functionality in the era of spectrum sensing. Digit. Signal Process. **119**, 103135 (2021)
3. H. Griffiths, L. Cohen, S. Watts, E. Mokole, C. Baker, M. Wicks, S. Blunt, Radar spectrum engineering and management: technical and regulatory issues. Proc. IEEE **103**, 85–102 (2015)
4. H. T. Hayvaci , B. Tavli, Spectrum sharing in radar and wireless communication systems: a review, in *Proc. Int. Conf. Electromagnetics in Advanced Applications*, pp. 810-813 (2014)
5. J. M. Chapin, Shared spectrum access for radar and communications (SSPARC), *Defense Advanced Research Projects Agency*, Arlington, VA, Tech. Rep. DARPA BAA -13 -24, (2013)
6. A.R. Chiriyath, B. Paul, D.W. Bliss, Radar-communications convergence: coexistence, cooperation, and co-design. IEEE Trans. Cogn. Commun. Netw. **3**(1), 1–12 (2017)

7. S.D. Blunt, E.S. Perrins (eds.), *Radar and communication spectrum sharing, stevenage* (Institution of Engineering and Technology, U.K, 2018)
8. F. Liu, C. Masouros, A. Li, T. Ratnarajah, J. Zhou, MIMO radar and cellular coexistence: a power-efficient approach enabled by interference exploitation. IEEE Trans. Signal Process. **66**(14), 3681–3695 (2018)
9. A. F. Martone, K. Ranney, and K. Sherbondy, Genetic algorithm for adaptable radar bandwidth, in Proc. *IEEE Radar Conference*, Philadelphia, PA, (2016)
10. A. Hassanien, M.G. Amin, E. Aboutanios, B. Himed, Dual-function radar communication systems: a solution to the spectrum congestion problem. IEEE Signal Process. Mag. **36**(5), 115–126 (2019)
11. A. Hassanien, M.G. Amin, Y.D. Zhang, F. Ahmad, Signaling strategies for dual-function radar communications: an overview. IEEE Aerosp. Electron Syst. Mag. **31**, 36–45 (2016)
12. L. Zheng, M. Lops, Y.C. Eldar, X. Wang, Radar and communication coexistence: an overview: a review of recent methods. IEEE Signal Process. Mag. **36**(5), 85–99 (2019)
13. J.A. Zhang et al., An overview of signal processing techniques for joint communication and radar sensing. IEEE J. Sel. Topics Signal Process. **15**(6), 1295–1315 (2021)
14. F. Liu, C. Masouros, A.P. Petropulu, H. Griffiths, L. Hanzo, Joint radar and communication design: applications state-of-the-art and the road ahead. IEEE Trans. Commun. **68**(6), 3834–3862 (2020)
15. A. Hassanien, M.G. Amin, Y.D. Zhang, F. Ahmad, Phase modulation based dual-function radar-communications. IET Radar Sonar Navig. **10**(8), 1411–1421 (2016)
16. A. Hassanien, M.G. Amin, Y.D. Zhang, F. Ahmad, Dual-function radar-communications: information embedding using sidelobe control and waveform diversity. IEEE Trans. Signal Process. **64**(8), 2168–2181 (2016)
17. S.D. Blunt, P. Yatham, J. Stiles, Intrapulse radar-embedded communications. IEEE Trans. Aerosp. Electron. Syst. **46**(3), 1185–1200 (2010)
18. M.J. Nowak, Z. Zhang, L. LoMonte, M. Wicks, Z. Wu, Mixed-modulated linear frequency modulated radar-communications. IET Radar Sonar Navig. **11**(2), 313–320 (2017)
19. C. Sahin, J. G. Metcalf, A. Kordik, T. Kendo, T. Corigliano, Experimental validation of phase-attached radar/communication (PARC) waveforms: radar performance, in proc. *International Radar Conference*, Oklahoma City, (2018)
20. S. D. Blunt, M. R. Cook, J. Stiles, Embedding information into radar emissions via waveform implementation, in *Proc. Int. Waveform Diversity and Design Conf.*, pp. 195-199 (2010)
21. M. Nowak, M. Wicks, Z. Zhang, Z. Wu, Co-designed radar-communication using linear frequency modulation waveform. IEEE Aerosp. Electron. Syst. Mag. **31**, 28–35 (2016)
22. C. Sahin, J. Jakabosky, P. M. McCormick, J. G. Metcalf, S. D. Blunt, A novel approach for embedding communication symbols into physical radar waveforms, in *Proc. IEEE Radar Conference*, pp. 1498-1503, (2017)
23. D. Gaglione, C. Clemente, C.V. Ilioudis, A.R. Persico, I.K. Proudler, J.J. Soraghan, A. Farina, Waveform design for communicating radar system using fractional Fourier transform. Digit. Signal Process. **80**, 57–69 (2018)
24. W.A. Gardner, W.A. Brown, C.-K. Chen, Spectral correlation of modulated signals: part II—digital modulation. IEEE Trans. Commun. **35**(6), 595–601 (1987)
25. A. Hassanien, E. Aboutanios, M.G. Amin, G.A. Fabrizio, A dual-function MIMO radar-communication system via waveform permutation. Digit. Signal Process. **83**, 118–128 (2018)
26. I. P. Eedara, M. G. Amin, and A. Hassanien, Analysis of communication symbol embedding in FH MIMO radar platforms, in proc. *IEEE Radar Conference*, Boston, USA, Apr. 22-26, (2019)
27. X. Wang, A. Hassanien, M.G. Amin, Dual-function MIMO radar communications system design via sparse array optimization. IEEE Trans. Aerosp. Electron. Syst. **55**(3), 1213–1226 (2019)
28. W. Baxter, E. Aboutanios, A. Hassanien, Joint radar and communications for frequency-hopped MIMO systems. IEEE Trans. Signal Process. **70**, 729–742 (2022)
29. E. BouDaher, A. Hassanien, E. Aboutanios, M.G. Amin, Towards a dual-function MIMO radar-communication system. IEEE Radar Conf. RadarConf **2016**, 1–6 (2016)
30. F. Liu, C. Masouros, A. Li, H. Sun, L. Hanzo, MU-MIMO communications with MIMO radar: from co-existence to joint transmission. IEEE Trans. Wirel. Commun. **17**(4), 2755–2770 (2018)
31. B.K. Chalise, M.G. Amin, B. Himed, Performance tradeoff in a unified passive radar and communications system. IEEE Signal Proc. Lett. **24**(9), 1275–1279 (2017)
32. B. K. Chalise , B. Himed, Performance tradeoff in a unified multi-static passive radar and communication system, in proc. *IEEE Radar Conference*, Oklahoma City, (2018)
33. B.K. Chalise, M.G. Amin, Performance tradeoff in a unified system of communications and passive radar: a secrecy capacity approach. Digit. Signal Process. **82**, 282–293 (2018)
34. T.W. Tedesso, R. Romero, Code shift keying based joint radar and communications for EMCON applications. Digit. Signal Process. **80**, 48–56 (2018)
35. Y. Dong, G.A. Fabrizio, M.G. Amin, Dual-functional radar waveforms without remodulation, in *Proc IEEE Radar Conf*, Boston, (2019)
36. M. G. Amin, Y. Dong, G. A. Fabrizion, Scheduling data embedding in dual function radar networks, in proc. *European Signal Processing Conf. (EUSIPCO 2019)*, Spain, (2019)
37. B. K. Chalise, M. G. Amin, G. Fabrizio, Multi-pulse processing of dual function radar waveforms without remodulation, in *EEE International Radar Conference*, Washington D.C., (2020)
38. A. Berni, W. Gregg, On the utility of chirp modulation for digital signaling. IEEE Trans. Commun. **21**(6), 748–751 (1973)
39. M.A. Richards, J.A. Scheer, W.A. Holm, *Principles of Modern Radar, Vol 1: Basic Principles*, Scitech Publishing, Inc., (2010)
40. K. Magowe, A. Giorgetti, K. Sithamparanathan, X. Yu, Accurate analysis of weighted centroid localization. IEEE Trans. Cognit. Comm. Netw. **5**(1), 153–164 (2019)
41. W.G. Bulgren, On representations of the doubly non-central F distribution. J. Am. Stat. Assoc. **66**, 84 (1971)
42. I.S. Gradshteyn, I.M. Ryzhik, *Table of Integrals, Series, and Products* (Academic Press, 2000)

43. X. Ouyang, J. Zhao, Orthogonal chirp division multiplexing. IEEE Trans. Commun. **64**(9), 3946–3957 (2016)
44. R. Bomfin, M. Chafii, G. Fettweis,Performance assessment of orthogonal chirp division multiplexing in MIMO space time coding, in *Proc. IEEE 2nd 5G World Forum (5GWF)*, Dresden, Germany, 30 (2019)
45. S. Guruacharya, B.K. Chalise, B. Himed, MAP ratio test detector for a radar system. IEEE Trans. Signal Process. **69**, 573–588 (2020)
46. G. Arfken, Confluent hypergeometric functions, *13.6 in Mathematical Methods for Physicists*, 3rd ed. Orlando, FL, Academic Press, pp. 753-758, (1985)

Publisher's Note